Available online at www.sciencedirect.com

ScienceDirect

ELSEVIER

Deep-Sea Research II 53 (2006) 2656–2683

DEEP-SEA RESEARCH
PART II

www.elsevier.com/locate/dsr2

Spring phytoplankton bloom and associated lower trophic level food web dynamics on Georges Bank: 1-D and 2-D model studies

Rubao Ji[a,*], Changsheng Chen[b], Peter J.S. Franks[c], David W. Townsend[d], Edward G. Durbin[e], Robert C. Beardsley[f], R. Gregory Lough[g], Robert W. Houghton[h]

[a] *Department of Biology, Woods Hole Oceanographic Institution, MS# 33, Redfield 1-32, Woods Hole, MA 02543, USA*
[b] *The School for Marine Science and Technology, University of Massachusetts Dartmouth, New Bedford, MA 02744, USA*
[c] *Integrative Oceanography Division, Scripps Institution of Oceanography, University of California, San Diego, La Jolla, CA 92093-0218, USA*
[d] *School of Marine Sciences, University of Maine, 5741 Libby Hall, Orono, ME 04469, USA*
[e] *Graduate School of Oceanography, University of Rhode Island, South Ferry Rd, Narragansett, RI 02882, USA*
[f] *Department of Physical Oceanography, Woods Hole Oceanographic Institution, Woods Hole, MA 02543, USA*
[g] *Northeast Fisheries Science Center, National Marine Fisheries Service, NOAA, Woods Hole, MA 02543, USA*
[h] *Lamont Doherty Earth Observatory of Columbia University, Palisades, NY 10964, USA*

Accepted 28 August 2006

Abstract

A coupled biological–physical model was developed and tested in one-dimensional (1-D, vertical) and two-dimensional (2-D, cross-sectional) domains to examine the spring phytoplankton bloom and associated lower trophic level food web dynamics on Georges Bank (GB). The biological model consists of nine compartments: dissolved inorganic nutrients (nitrate, ammonium and silicate), phytoplankton (large and small size classes), zooplankton (large and small size classes), and detrital organic nitrogen and biogenic silica. The 1-D model results showed that in the shallow central bank, the timing and duration of spring blooms are closely linked to the light intensity and its downward penetration, while the intensity of blooms is regulated by initial nutrient concentrations and zooplankton grazing pressure. In the deeper flank area, the bloom dynamics is directly controlled by the seasonal development of stratification. The interactions between the shallow and deep regions of the bank were examined by a 2-D model, which showed that the cross-sectional gradients of biological quantities were caused mainly by the shallow-deep topographic transition and tidal mixing. Between the shallow and deep regions, a possible phytoplankton maximum concentration area was seen in the model at the time before the formation of the tidal-mixing front. Once the tidal-mixing front was established during late spring, the model showed a relatively high concentration of phytoplankton near the front as the result of the tidally driven up-front nutrient flux. Both the 1-D and 2-D models captured the basic seasonal cycles of the nutrients and phytoplankton

---

*Corresponding author. Tel.: +1 508 289 2986; fax: +1 508 457 2134.
E-mail address: rji@whoi.edu (R. Ji).

0967-0645/$ - see front matter
doi:10.1016/j.dsr2.2006.08.008

in the central bank, but failed to reproduce those patterns in the deep flank regions, where horizontal advection might play a significant role.

Keywords: Phytoplankton; Algal blooms; Food webs; Dynamics; Modeling

1. Introduction

Our previous understanding of the spring phytoplankton bloom and associated nutrient and phytoplankton dynamics on Georges Bank (GB) are mainly based on retrospective studies (e.g., Cura, 1987; O'Reilly et al., 1987). Those studies suggested that spring phytoplankton blooms generally occur in the well-mixed shallow region of GB (<60 m) during late winter and early spring (mainly in March), but develop in the deeper flank regions (60–100 m) in late spring and early summer (around April), when the water starts to be vertically stratified. The blooms usually decline rapidly by late April and/or early May along with the depletion of nutrients on the bank.

This general seasonal pattern of the phytoplankton bloom was challenged by recent observational evidence from the US GLOBEC/GB multi-year interdisciplinary surveys (Townsend and Thomas, 2001, 2002) and ocean-color data (Thomas et al., 2003). Their studies clearly showed significant inter-annual variation in the timing, duration, and location of spring blooms on GB. For example, a strong phytoplankton bloom developed in the central portion of the bank in May 1997—about 2 months later than that described by the general pattern. In 1999, the bloom started in February in the central bank, continued to intensify until April followed by a decrease in May, and then reoccurred in the mid-bank region between the 40- and 70-m isobaths. Many biological and physical factors may contribute to this inter-annual variation, including changes in phytoplankton species composition, light intensity/attenuation, nutrient concentrations, zooplankton grazing pressure, vertical mixing, and horizontal advection.

Biological–physical coupled models provide unique tools to understand phytoplankton dynamics and have been applied in various coastal oceans, such as the Bering Sea shelf (Eslinger and Iverson, 2001), the coastal North Pacific (Eslinger et al., 2001; Yoshie et al., 2003), and the coastal Mediterranean Sea (Lacroix and Nival, 1998). On GB, previous modeling studies (Franks and Chen, 1996b, 2001; Klein, 1987; Lewis et al., 1994) have been mostly focused on the process-oriented explorations of the impacts of physical–biological interactions on the short-term growth and variability of phytoplankton biomass under tidal and wind forcings. A three-compartment nutrient–phytoplankton–zooplankton (NPZ) model was widely used, and nitrogen was considered to be the only limiting nutrient on phytoplankton growth in those models. This simplification may not be sufficient to describe the spring blooms and associated lower trophic level food web dynamics on GB, where both silicon and nitrogen are presumably important limiting nutrients, and considerable temporal variation of phytoplankton species composition exists (Townsend and Thomas, 2002). Therefore, a simple NPZ model might not be suitable for the study of the seasonal and inter-annual variability of the lower-trophic food web dynamics on GB. This leads to the development of the model used in this study, which includes both nitrogen and silicate as potential limiting nutrients and partitions plankton into different size classes.

The objective of this modeling study is to examine the relative importance of various biological–physical processes in controlling the spring blooms and associated lower-trophic-level food web dynamics (e.g., seasonal and inter-annual variation) on GB. Biological processes include bottom-up (light and multi-nutrient limitation) and top–down (zooplankton grazing) control, whereas physical processes include vertical stratification and tidal mixing. A nine-compartment lower-trophic-level food web model was coupled into 1-D (vertical in space) and 2-D (cross-sectional in space) versions of the finite-difference coastal ocean model (ECOM-si, Blumberg, 1994). The numerical experiments were conducted with the 1-D model focus on local forcings (mixing, cooling/heating) and the 2-D model on the tidally induced cross-section exchange and seasonally formed tidal-mixing front.

2. Physical model

The 1-D physical sub-model is adapted from Chen et al. (2002). It is a spatially simplified

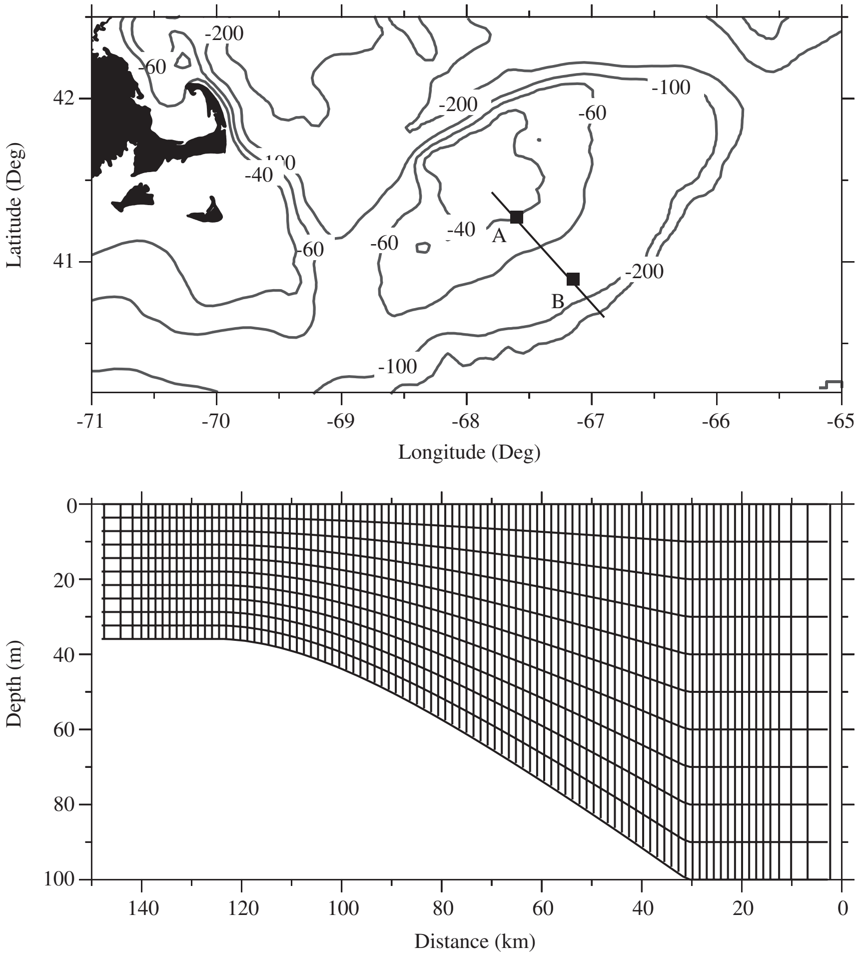

Fig. 1. Top panel: Georges Bank and its bathymetry. The 1-D model was applied at Sites A and B. Site A is 40 m deep, representing the well-mixed region; Site B is 80 m deep, representing the seasonally stratified region. The 2-D model was conducted along the section connecting Sites A and B. Bottom panel: The numerical model grid for the 2-D model. The grid is plotted every five points in the vertical and every three in the horizontal. Horizontal resolution is 500 m near and across the bank and increase linearly over an interval of 30 grid points to 11.96 km away from the region of interest.

ECOM-si 3-D model with a 5×5 horizontal model grid, in which all biological and physical variables are set equal to each other. Vertically, a uniform σ coordinate grid is used, with a resolution of $\Delta\sigma = 0.0196$ (51 points in the vertical). Two sites with different water depths are modeled in the 1-D case (Fig. 1, top panel). The site with 40 m water depth (Site A) represents the well-mixed area, and the site with 80 m water depth (Site B), the seasonally stratified area. The Mellor and Yamada (1982) level-2.5 turbulence closure scheme is used for the turbulent mixing of momentum and tracers. Considering the difference of tidal mixing over the shallow and deep areas of the bank, background-mixing coefficients of 10^{-3} and $10^{-4}\,\mathrm{m}^2\,\mathrm{s}^{-1}$ were used for Sites A and B, respectively.

The configuration of the 2-D model features a cross-isobath section with water depth varying from 100 m on the southern flank to 36 m on the top of the bank (Fig. 1, bottom panel). The vertical coordinate system is the same as that used in the 1-D model, with a resolution of $\Delta\sigma = 0.0196$ (51 points in the vertical). This resolution corresponds to a maximum vertical depth of 2 m off the bank and <1 m on the top of the bank. A non-uniform horizontal grid is used in the cross-bank direction. The horizontal resolution is 500 m near and across the bank and increases linearly over an interval of 30 grid points to 11.96 km outside the immediate domain (shown in Fig. 1). The time step is 110.4 s, corresponding to 405 time steps over an M_2 (12.42 h) tidal cycle. The M_2 tidal forcing is specified

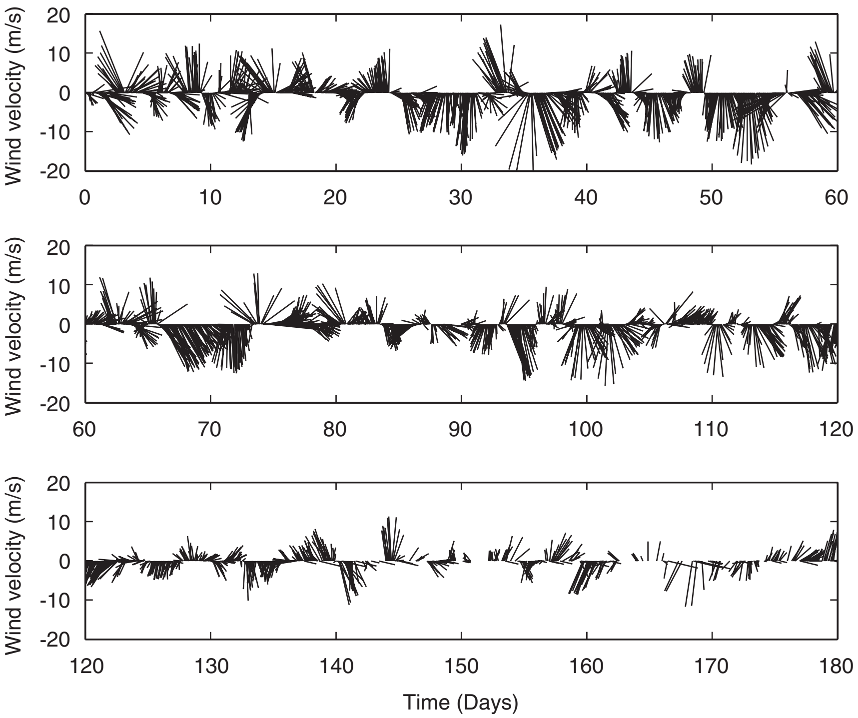

Fig. 2. Time series of wind velocity and direction on the southern flank of Georges Bank from 1 January to 30 June 1999. The data are extracted from the MM5 model developed for GoM/GB region (Chen et al., 2005).

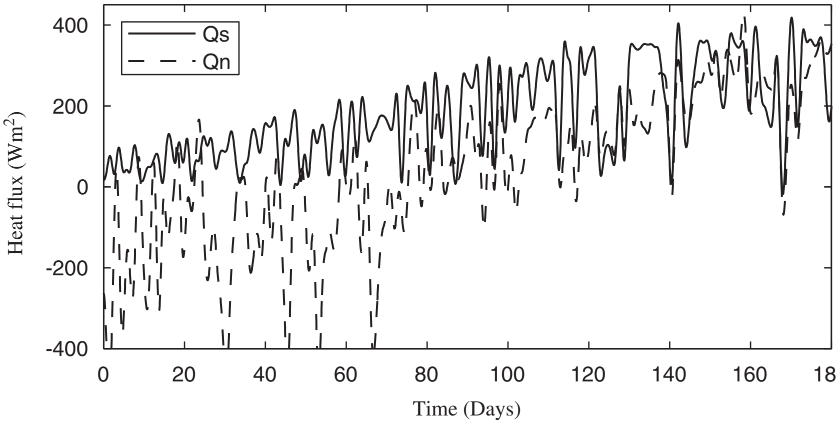

Fig. 3. The low-pass (48 h) filtered short-wave (Qs) heat flux and net (Qn) heat flux on the southern flank of Georges Bank from 1 January to 30 June, 1999. The data are extracted from the MM5 model developed for GOM/GB region (Chen et al., 2005).

at the southern open boundary, and a gravity wave radiation condition is applied at the northern open boundary.

The surface and bottom momentum fluxes were computed from surface wind and near-bottom currents as described in Chen et al. (2002). For temperature, the surface boundary condition was computed based on a prescribed surface heat flux. Interested readers are referred to Chen et al. (2003a) for a detailed description for computing the surface heat flux, vertical profile of shortwave radiation, and surface/bottom temperature boundary conditions for the GB ECOM-si model. Surface heat flux and wind data were obtained from a Gulf of Maine (GOM) regional mesoscale meteorological model MM5 (Chen et al., 2005). Figs. 2 and 3 show,

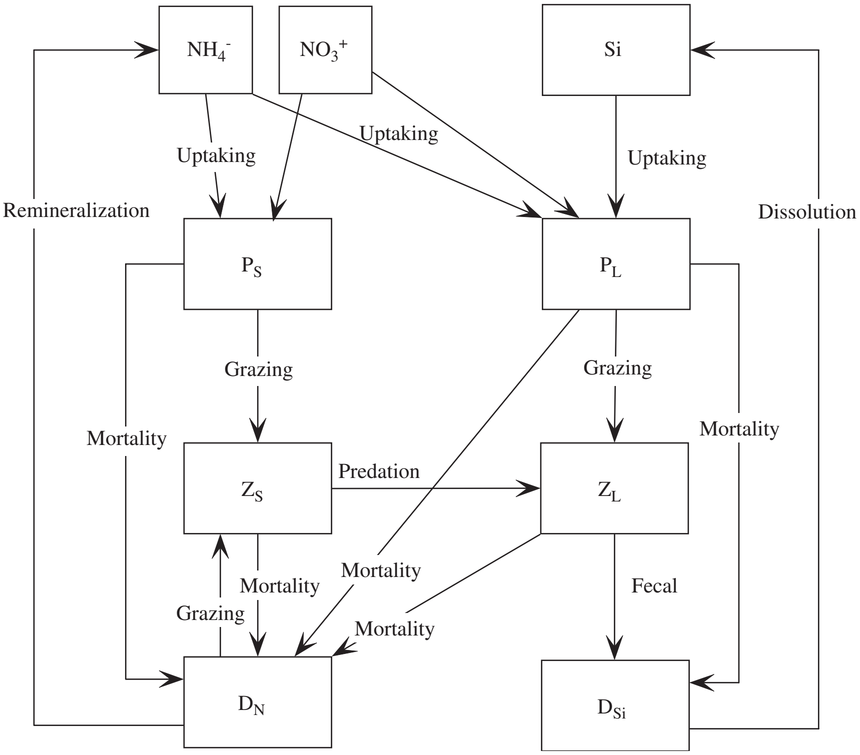

Fig. 4. Schematic of the lower-trophic-level food web model used in this study. The model consists of nine compartments including nitrate (NO_3^-), ammonium (NH_4^+), silicate (Si), small phytoplankton (P_S), large phytoplankton (P_L), small zooplankton (Z_S), large zooplankton (Z_L), detrital organic nitrogen (D_N) and detrital biogenic silica (D_{Si}). Arrows represent fluxes between different compartments.

respectively, the resulting time series of wind velocity and direction and the low-pass (48 h) filtered shortwave (Qs) and net (Qn) heat fluxes on the southern flank of GB during the first 180 days of 1999.

3. Biological model

The biological model was developed based on the ecosystem dynamics observed in the US GLOBEC/GB interdisciplinary surveys (e.g., Townsend and Thomas, 2002). This model consists of nine compartments including nutrients (nitrate, ammonium and silicate), phytoplankton (large and small size classes), zooplankton (large and small size classes), detrital organic nitrogen and biogenic silica. The schematic of the model is shown in Fig. 4.

In the biological model, two classes of phytoplankton were selected, distinguished by their size and dependence on silicate. The small-sized phytoplankton represents nano- and pico-phytoplankton, usually flagellates. The growth of phytoplankton in this size class is limited primarily by nitrogen and light. The large-sized phytoplankton is explicitly modeled as diatoms, and its growth is potentially limited by light, nitrogen, and silicate. The zooplankton communities on GB and the surrounding region are dominated in numbers and biomass by copepods *Calanus finmarchicus*, *Pseudocalanus* spp., *Paracalanus parvus*, *Centropages typicus*, *Centropages hamatus*, and *Oithona similis* (Davis, 1987). In this model, the large-sized zooplankton represents the aggregation of those species, whereas the small-sized zooplankton represents mainly heterotrophic protozoans. Caution needs to be taken here: due to the lack of higher trophic level regulations on the zooplankton compartments, the simulation of zooplankton is difficult to validate. Instead, the large and small zooplankton function as dynamic closure terms to balance and maintain the stability of the lower trophic level food web model. The detailed equations that describe the source and sink terms of each compartment are listed in the Appendix A. The selection of formulae and parameters for the major biological processes is explained next.

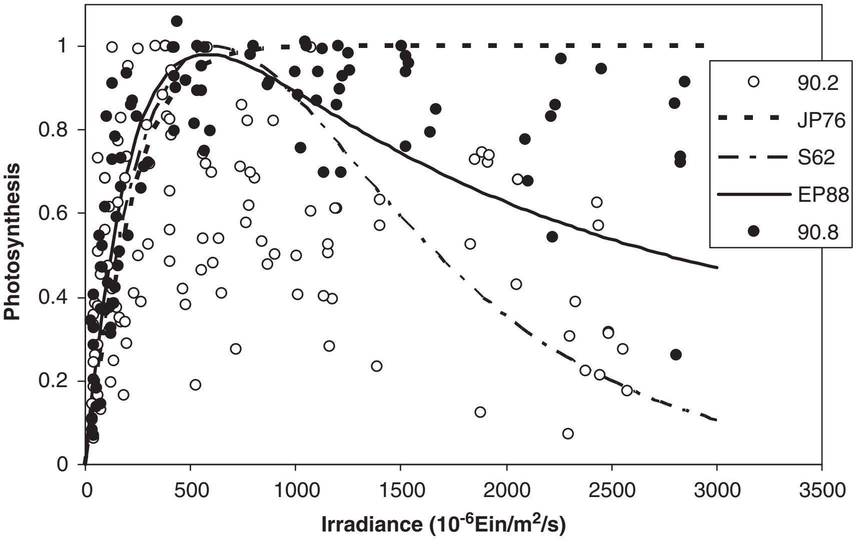

Fig. 5. Photosynthesis vs. irradiance. The data are from D. Townsend's field measurements in Massachusetts Bay during February 1990 (blue diamonds) and August 1990 (red filled circles). Photosynthetic rate is normalized to the maximum rate. Three functions are applied to fit the data. Orange line: (JP76: Jassby and Platt, 1976); Blue line: (EP88: Eilers and Peeters, 1988); Black line: (S62: Steele, 1962).

3.1. Light limitation

Many mathematical models have been proposed to describe the photosynthesis–irradiance (P/I) relationship (Steele, 1962; Jassby and Platt, 1976; Platt et al., 1980; Falkowski and Wirick, 1981; Mergard et al., 1984; Eilers and Peeters, 1988; Pahl-Wostl and Imboden, 1990; Janowitz and Kamykowski, 1991). The experiments carried out in Massachusetts Bay in February and August 1990 provided the empirical evidence for an approximation of the P/I relationship for the phytoplankton community for GB (and the surrounding GOM) in this model (Fig. 5). The data showed that photoinhibition is more likely to occur in February than in August. Vertically, samples from deeper stations were more subject to photoinhibition. A normalized photosynthetic rate (normalizing the photosynthetic rate to its maximum value for each station) is plotted against irradiance, and three functions were tested to fit the observations, including a hyperbolic tangent function (not including photoinhibition, Jassby and Platt, 1976), Steele's function with light saturation and inhibition (Steele, 1962) and a physiology-based function (Eilers and Peeters, 1988) that has the form

$$P^B = \frac{I}{aI^2 + bI + c},$$

where P^B is the instantaneous photosynthesis rate normalized to the chlorophyll biomass B. I represents photosynthesis available radiation (PAR). a, b and c are parameters related to optimal light intensity and maximum photosynthetic rate. The hyperbolic tangent function seems to fit the data better in the summer (August), while Steele's function fits better in the spring (February). Eilers and Peeter's function falls in between, and this function was adopted in the baseline model run. As we can see, the variance of the observed data is significant, so that the choice of parameters for the light function is quite arbitrary. After comparing these three different P/I relationships described above, only the model results with the Eilers and Peeter's function are presented here.

3.2. Nutrients

Nitrogen was believed to be the primary limiting factor that influences the formation and duration of spring blooms on GB. Based on observations, the timing of nitrate depletion generally coincides well with the spring bloom (O'Reilly et al., 1987). Recent US GLOBEC/GB field measurements (Townsend and Thomas, 2001, 2002) revealed that the timing and duration of spring bloom also might be related to the availability of silicate in the water column. In all 3 years (1997–1999), the central bank was characterized by a low concentration of silicate in February, with the lowest in 1999. Diatom blooms were coincident with a rapid decrease of silicate in the central bank in all 3 years of the field measurements, suggesting that nitrogen may not be the only limiting nutrient that controlled the spring bloom. This issue will be addressed further in the results and discussion sections.

Nutrient limitation follows Liebig's law of the minimum: only the most limiting nutrient controls phytoplankton growth rate. Nitrogen uptake by phytoplankton is partitioned between ammonium and nitrate. The inhibition effect of ammonium concentration on nitrate uptake has been taken into consideration by using the same approach as Frost and Franzen (1992). A standard Michaelis–Menten equation is used for the silicate uptake by large phytoplankton. The half-saturation constant is set at 2.0 μmol/l in the model, which is at the lower bound of values described in Paasch (1973) (2.0–4.0 μmol/l).

3.3. Phytoplankton

Phytoplankton biomass is determined by the balance between growth, physiological or non-grazing mortality, and grazing loss. The growth of phytoplankton is primarily controlled by the specific growth rate, which is the maximum growth rate modulated by temperature and nutrient/light limitation. Phytoplankton mortality, specified as physiological death and subsequent lysis of phytoplanktonic cells, results from a number of factors, including parasitic attack by viruses, bacteria and fungi or exposure to physiological extremes of light, temperature, nutrient concentration, and toxic substances (Reynolds, 1984). The grazing loss of phytoplankton by zooplankton is controlled by the grazing rate, which is related with the concentration of phytoplankton and is described below.

3.4. Zooplankton

Zooplankton biomass is controlled by the grazing and mortality terms. For large zooplankton, both small zooplankton and large phytoplankton are food sources. Although Townsend and Thomas (2002) suggested that large zooplankton might prefer small zooplankton (heterotrophic protozoans) over large phytoplankton as a food source on GB, a feeding preference is not considered in this model. This is mainly due to the difficulty of parameterizing the preference in the absence of sufficient data. Also, based on a trial model run in this study, the biomass of small zooplankton is low during the modeled time period, suggesting a secondary role played by small zooplankton.

Grazing of large zooplankton on large phytoplankton, small zooplankton on small phytoplankton, and large zooplankton on small zooplankton all follow the Ivlev (1961) function. A constant fraction of the ingested food is assimilated into the biomass, with the non-assimilated fraction rejected as detrital organic matter. An important assumption for silicon flux during large zooplankton grazing on large phytoplankton is that copepods do not digest the diatom frustules and thus the siliceous parts of diatoms are directly deposited into the detrital pool (Scavia et al., 1988; Chen et al., 2002).

Zooplankton mortality has a quadratic form, i.e. the mortality rate is linear to its biomass. This treatment was proposed by Steele and Henderson (1992) to reduce the oscillation inherent to the system, and has been adapted as a convenient mathematical maneuver in many modeling exercises (e.g., Denman and Gargett, 1995; Fasham, 1995; Chen et al., 2002; Ji et al., 2002). Biologically, this quadratic form also represents the limit on the numerical response of zooplankton by the carrying capacity of the system, and has been supported by some observational evidence in terms of density-dependent mortality rates for some open-ocean zooplankton species (Ohman and Hirche, 2001).

3.5. Detritus

The detrital compartments play the role of "buffers" in this model: all the dead material from phytoplankton and zooplankton, as well as the egesta during the grazing process, goes into the detrital compartments; the remineralization of detritus by bacteria recycles a part of those nutrients back to the system. Two detrital compartments, detrital nitrogen and biogenic silica, are modeled separately instead of one single compartment. This treatment is adapted from the nine-component model developed by Chen et al. (2002). Biologically, if we use a single detrital component, it is difficult to resolve the ratio of nitrogen to silicon from the total concentration of detritus, since this ratio varies with multiple factors related to the mortality of phytoplankton, zooplankton, and the assimilation rate of zooplankton.

Ammonium is modeled as a recycled nutrient, with the only source being detrital nitrogen. This is far more simplified than the real situation, where processes such as zooplankton excretion can produce ammonium instantaneously. However, this simplification allows the regeneration process to be parameterized into one single temperature-dependent decomposition rate, without detailing the bacterial processes and different chemical steps. Also, an implicit treatment of the microbial food web is incorporated into this model by allowing small zooplankton to graze directly on detrital nitrogen.

Dissolved organic matter is not modeled explicitly for the following two reasons: (1) it is implicitly included in the detrital component, by allowing phytoplankton exudation, zooplankton excretion and egestion to transfer to detritus, and (2) the processes that control the concentration of dissolved organic matter are poorly known. For example, labile compounds of dissolved organic matter can be degraded by bacteria and transferred to higher trophic levels via the microbial food web, while more refractory compounds are remineralized over time scales ranging from months to centuries (Druffel et al., 1992).

3.6. Other issues

There are two "currencies" coexisting in this model, nitrogen and silicon. All the silicon-related processes involve large phytoplankton (diatoms). The exchange of these two "currencies" is via a constant N:Si ratio of diatoms. In reality, this ratio varies with species composition and light conditions. The average value is close to 1.0 with a factor of 3 variation (Brzezinski, 1985). A value of 1.5 is used in this model for the standard run. Phytoplankton is usually measured as the chlorophyll-*a* (Chl-*a*) concentration. To convert between nitrogen and Chl-*a* concentration, two ratios (C:N and C:Chl-*a* ratios) need to be determined. The C:N ratio is assumed to be the Redfield value, 6.6 (atom:atom). The C:Chl-*a* ratio for phytoplankton varies over a wide range. For a healthy, nutrient-sufficient diatom community, the ratio ranges from 21.5 to 46.6 (weight ratio) (Gallegos and Vant, 1996). Early studies (Strickland, 1960; Parsons et al., 1984) have shown variation of the C:Chl-*a* ratio from 23 to 79 during a diatom bloom, and an average value of 30 has been suggested. Both nutrient supplies and the light regime impact this ratio. Here, an average C:Chl-*a* ratio of 40 is used. Combining these two ratios gives a ratio, N (mmols):Chl-*a* (mg) of 0.5.

Estimation of biological parameters is often very difficult due to the complex nature of biological processes. Most of the parameters used in this model are either from observational data or literature. The parameters with no data support were tested with a "trial and error" method to give the best agreement with Chl-*a* concentration and the nitrogen fluxes supported by observational data. A sensitivity analysis also was conducted to identify those sensitive parameters.

4. Model results

4.1. The 1-D model results in shallow site (Site A)

The water temperature was vertically homogeneous throughout the modeled time period, from the beginning of January to the end of June (Fig. 6). The coldest water temperature (~4 °C) was not reached until March. The water started warming up by April, when temperatures ranged from 5 to 6 °C and then reached 12 °C by the end of June. Qualitatively, the model results agree well with observations of water temperature evolution over the top of GB (see Townsend and Thomas, 2002), providing a reasonable basic physical background for the biological model.

During the spring, the phytoplankton was dominated by the large size class. The model results showed a significant bloom starting from March and ending in middle April (Fig. 6). The total biomass reached 3.0–3.6 μmol N l^{-1}, equivalent to 6.0–7.2 μg Chl-*a*/l. Small phytoplankton constituted only a small fraction of the total biomass in early spring and started to grow during the end of May, and their biomass reached ~1.0 μmol N l^{-1} during June. The modeled temporal variation of species composition matches well with the general pattern observed on GB (O'Reilly et al., 1987; Townsend and Thomas, 2002).

The temporal variations of nutrient concentrations were closely related to the growth of phytoplankton. Nitrate concentration decreased from 5.0 μmol N l^{-1} in January to nearly depleted at the beginning of April, and remained low during the rest of the modeling period (Fig. 6). Ammonium concentration changed more irregularly due to the balance of decomposition of particulate organic nitrogen and phytoplankton uptake. It increased from January to

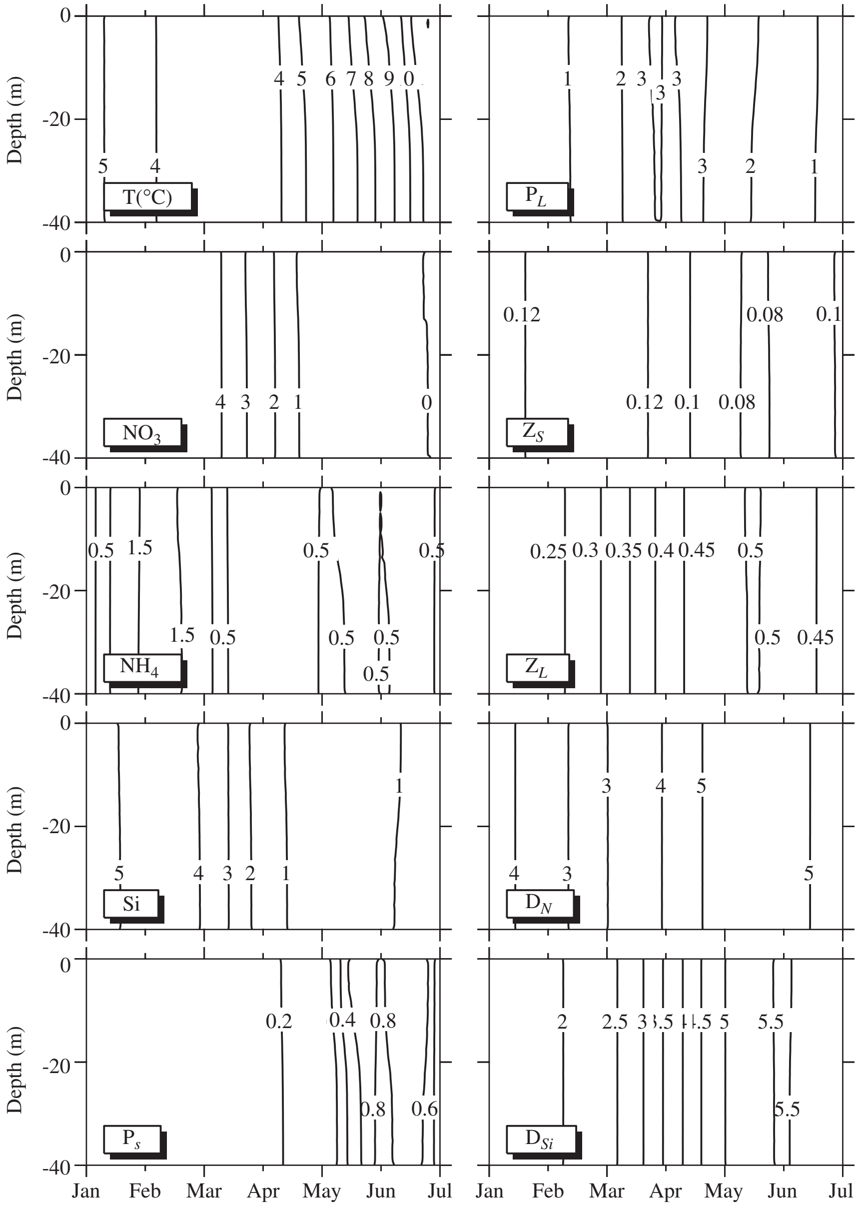

Fig. 6. Time sequence of the vertical distribution of model-predicted temperature (*T*), nitrate (NO_3^-), ammonium (NH_4^+), silicate (Si), small phytoplankton (P_S), large phytoplankton (P_L), small zooplankton (Z_S), large zooplankton (Z_L), detrital organic nitrogen (D_N) and detrital biogenic silica (D_{Si}) at Site A from January to June.

February from 0.2 to ~1.5 μmol N l^{-1}, and then gradually decreased to 1.0 μmol N l^{-1} in March. When diatoms started to bloom in March, ammonium was quickly consumed due to its preferential uptake over nitrate by phytoplankton. Silicate decreased from January to May from 5.0 μmol Si/l to near zero, due to the uptake by large phytoplankton. This was almost synchronous with the depletion of nitrate. During June, the silicate concentration increased again, partially due to the decrease of uptake by large phytoplankton during the post-bloom period. More importantly, the dissolution of biogenic silica increased with the rise of seawater temperature. Unlike silicate, nitrate is not able to recover without supply from outside of the system.

The biomass of large zooplankton increased 1 month after the increase of phytoplankton biomass (Fig. 6). The peak appeared during May with biomass >0.5 μmol N l^{-1}, then gradually decreased to 0.35 μmol N l^{-1} in June. Compared with large zooplankton, small zooplankton was less abundant, mainly due to the lack of small phytoplankton as food resource in the model. The biomass remained $<0.2\,\mu$mol N l^{-1} during the entire modeling period. Due to the grazing of large zooplankton, the biomass of small zooplankton decreased to the lowest level ($<0.1\,\mu$mol N l^{-1}) during May, whereas the biomass of small phytoplankton started to catch up at that time.

Both particulate organic nitrogen and biogenic silica increased from January to June (Fig. 6). Particulate biogenic silica increased more significantly than particulate nitrogen due to its slower decomposition. This pattern of increase indicates that, in general, the mass has been transferred from

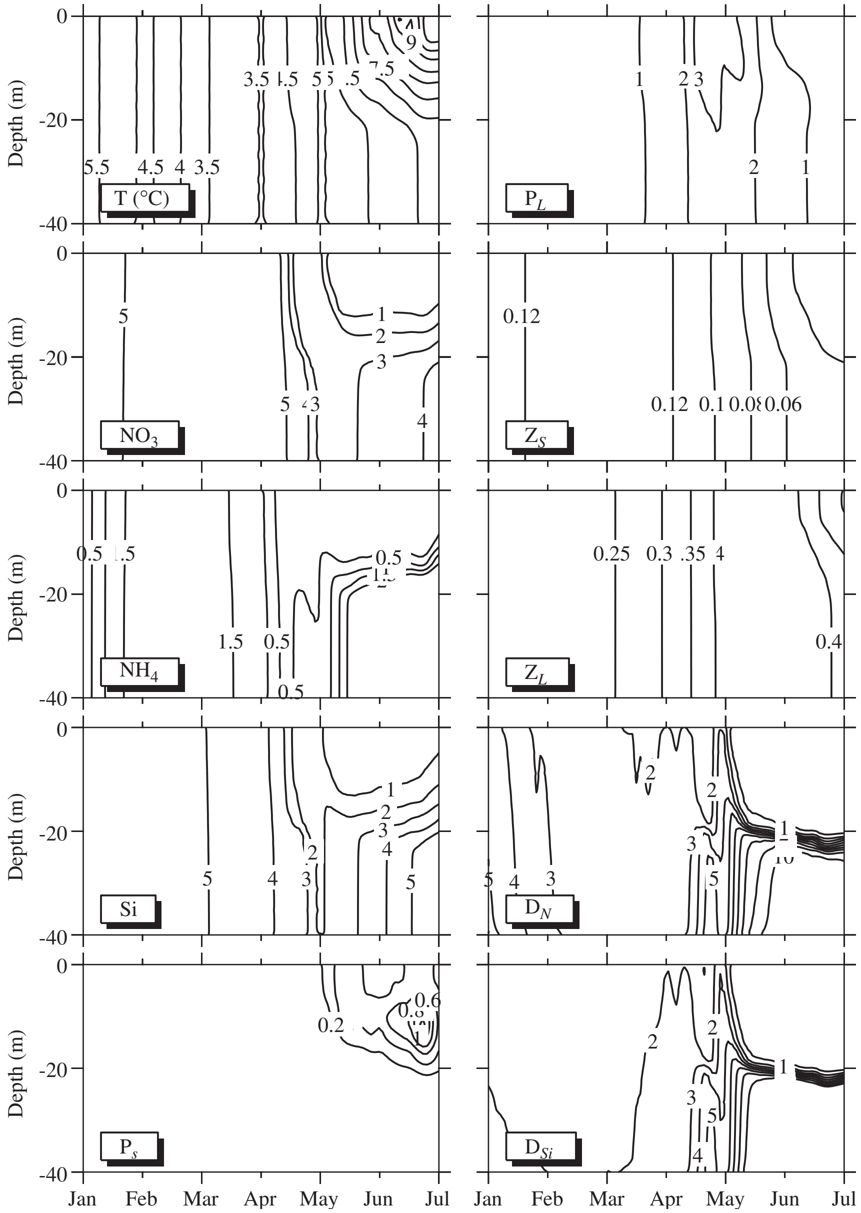

Fig. 7. Time sequence of the vertical distribution of model-predicted temperature (T), nitrate (NO_3^-), ammonium (NH_4^+), silicate (Si), small phytoplankton (P_S), large phytoplankton (P_L), small zooplankton (Z_S), large zooplankton (Z_L), detrital organic nitrogen (D_N) and detrital biogenic silica (D_{Si}) in the upper 40 m at Site B from January to June.

inorganic form to organic form as a result of the biological processes.

4.2. The 1-D model results in the deep site (Site B)

The water temperature was vertically homogeneous from the beginning of January to the middle of April (Fig. 7). A weak stratification started to develop and became intensified from May to June when the surface water temperatures were about 9–10 °C, whereas the water below 60 m remained cold with a temperature of 5–6 °C. The model simulated the evolution of water temperature structure very well, especially the timing of stratification.

In contrast with the well-mixed site, large phytoplankton did not bloom during March and early April (Fig. 7). Instead, a significant bloom occurred in the upper water column (<50 m) from the middle of April to the end of May. The biomass of large phytoplankton reached $>5.0\,\mu\mathrm{mol\,N\,l^{-1}}$ during the peak, though the duration was very short—about 10 days. The bloom declined after the beginning of June. The biomass of large phytoplankton in the surface layer (above 20 m) in June was less than $0.3\,\mu\mathrm{mol\,N\,l^{-1}}$, while in the subsurface (20–40 m deep), a weak phytoplankton band remained, probably due to combination of two factors: sinking of diatoms and increased subsurface diatom growth stimulated by the nutrient supply from deep water under the stratified layer. Small phytoplankton started to show very weak signs of growth during the middle of May; and their biomass reached ca. $1.0\,\mu\mathrm{mol\,N\,l^{-1}}$ by late June.

The nitrate concentration remained high from January to the middle of April, then decreased from $5.0\,\mu\mathrm{mol\,N\,l^{-1}}$ to near zero in the upper water column (<40 m) in less than a week, corresponding to the significant diatom bloom in the stratified region (Fig. 7). Ammonium concentration increased dramatically after January and remained very high ($>2\,\mu\mathrm{mol\,N\,l^{-1}}$) in the whole water column until mid-April. The surface ammonium concentration decreased quickly from mid-April and diminished during May and June, while the deeper waters (>40 m) kept a higher concentration of ammonium. The occurrence of high ammonium concentrations in the deep layer in this model is contradictory to the observations where concentration over $0.2\,\mu\mathrm{mol\,N\,l^{-1}}$ are rarely reported (Townsend and Thomas, 2002). This is probably due to the lack of nitrification in this model. Not surprisingly, the concentration of silicate showed a similar pattern of spatial and temporal variation as that of nitrate and ammonium, corresponding to the diatom bloom starting from mid April.

The large zooplankton biomass increased as phytoplankton biomass increased with a time lag of about 1 month (Fig. 7). Peak biomass occurred in May and early June with values of $0.4–0.5\,\mu\mathrm{mol\,N\,l^{-1}}$, then declined at the end of June. Small zooplankton was much less abundant due to the grazing of large zooplankton and lower concentration of small phytoplankton as food source.

Both particulate organic nitrogen and biogenic silica decreased in the entire water column from January to early April due to decomposition (Fig. 7). After mid-April, the stratification-stimulated bloom increased the flux from inorganic matter to organic matter. A high particulate organic nitrogen and biogenic silica concentration in the lower water column was observed due to sinking.

4.3. The 2-D model results

The water was vertically well mixed across the entire section before April, and did not show many interesting dynamics other than simple tidal-mixing between the shallow and deep areas. Therefore the 2-D model results presented here focus only on biological and physical features developed after April.

The water started to become weakly stratified in deeper flank region due to the increased surface heating in April (Fig. 8, top panel). Along with this stratification, we also can see the formation of multiple circulation cells across the section and a vertically non-uniform distribution of V, velocity, along with vertical secondary circulation cells near the deep-shallow transition zone (Fig. 8, bottom three panels). This circulation pattern changed further with the intensification of stratification during June (Fig. 9). The residual flow field showed a strong southwestward current jet in the along-bank direction and double circulation cells in the cross-bank direction north of the tidal-mixing front. The current jet had a maximum speed of about 12 cm/s at a subsurface depth of 10–15 m. Near the tidal-mixing front zone, two secondary circulation cells existed with a divergence near the surface and a convergence near the bottom. The water tended to converge toward the bank-edge of the tidal mixing front in the upper 10 m and then recirculate back in the deeper region (Fig. 9, bottom three panels). This depiction of the secondary circulation is very

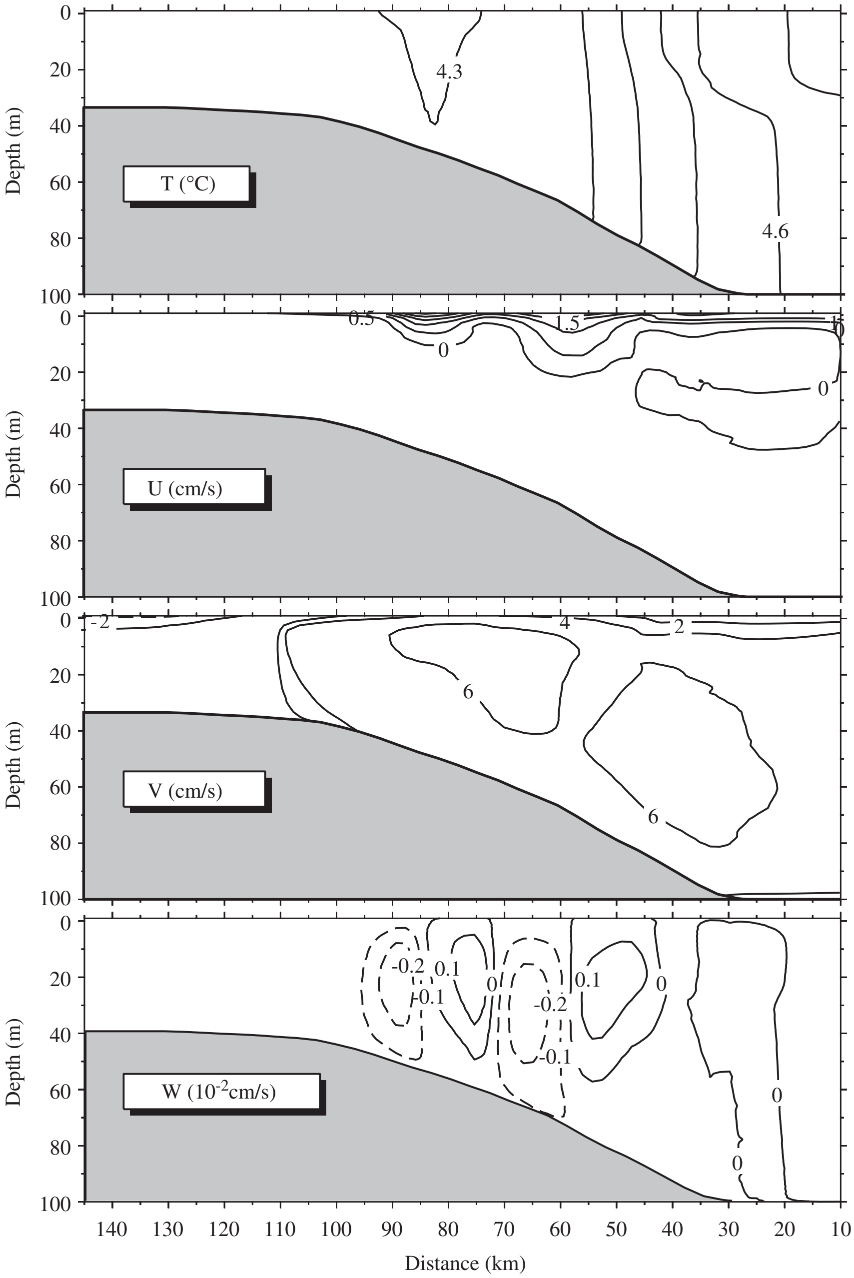

Fig. 8. Model-computed cross-isobath distribution of tidally averaged temperature (*T*), and cross-bank (U: positive on-bank), along-bank (V: positive out of the paper) and vertical (W: positive upward) velocities on the southern flank of GB on April 15, 1995.

similar to that suggested using semi-analytical diagnostic frontal models (Garrett and Loder, 1981; Chen and Beardsley, 2002). Those circulation features appear to significantly affect the biota exchange across the section.

For the biological variables, in order to focus on the nutrients and phytoplankton dynamics, only the distribution of nitrate, silicate, small phytoplankton and large phytoplankton are presented here. As shown in Fig. 10, the concentration gradients of phytoplankton and nutrients across the section have become well developed during April, resulting primarily from the earlier phytoplankton bloom in the shallow area as opposed to the deep region. The large phytoplankton increased to 2.7 μmol N l^{-1}, whereas nitrogen and silicate became

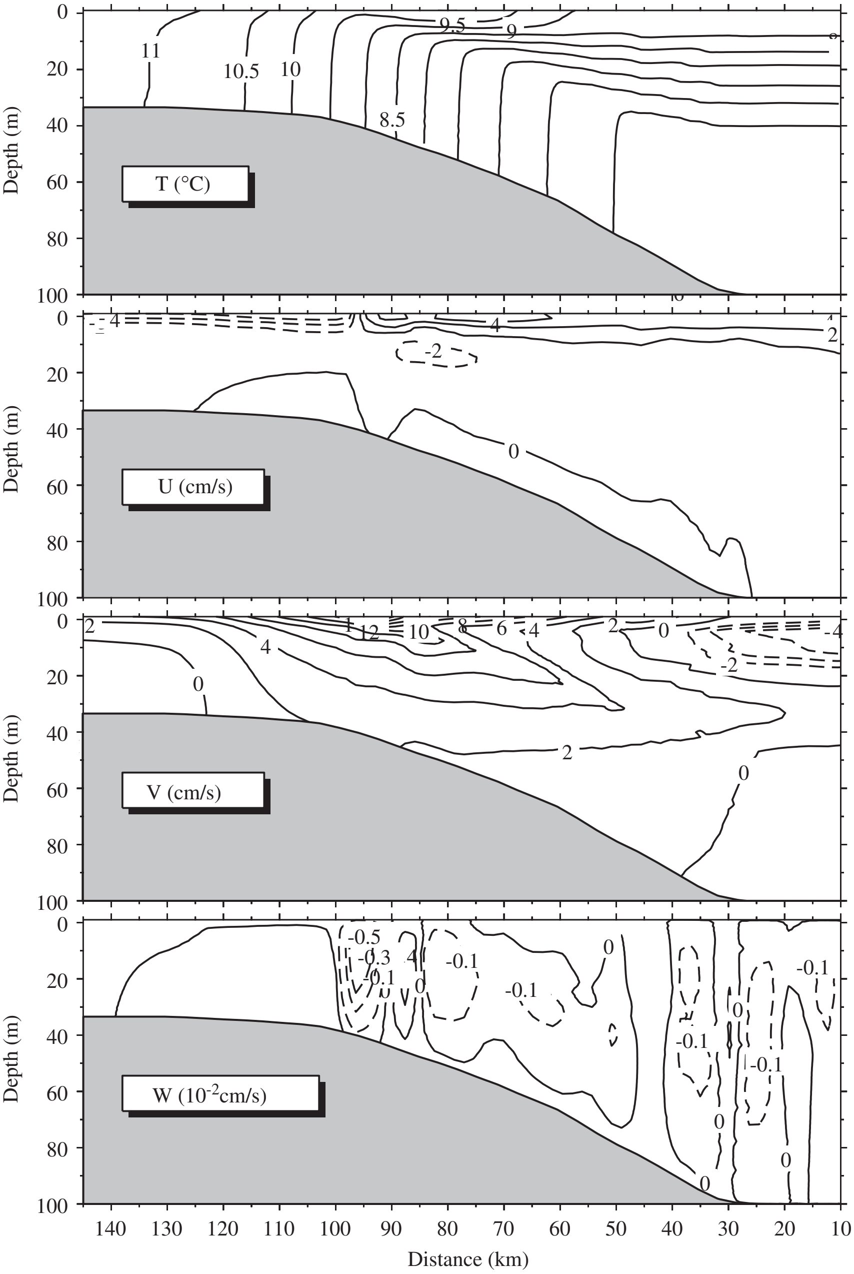

Fig. 9. Model-computed cross-isobath distribution of tidally averaged temperature (*T*), and cross-bank (U: positive on-bank), along-bank (V: positive out of the paper) and vertical (W: positive upward) velocities on the southern flank of GB on June 15, 1995.

almost depleted over the area shallower than 50 m. When the stratification fully developed in the deep region during June (Fig. 11), the large phytoplankton bloom declined to a concentration of $\sim 1.0\,\mu\mathrm{mol\,N\,l^{-1}}$ in the shallow area. Near the frontal zone, the concentration of phytoplankton was slightly higher due to nutrient supply from the deep nutrient-rich region by tidal mixing processes, as shown in the nitrate and silicate distributions. In the deep area, large phytoplankton showed a subsurface maximum layer caused by growth and sinking from the surface-mixing layer. Nitrate was depleted both in the shallow area and at the surface of the deep area, while an upward intrusion of deep nutrient-rich water was observed near the frontal zone with a water depth of 50–60 m. This

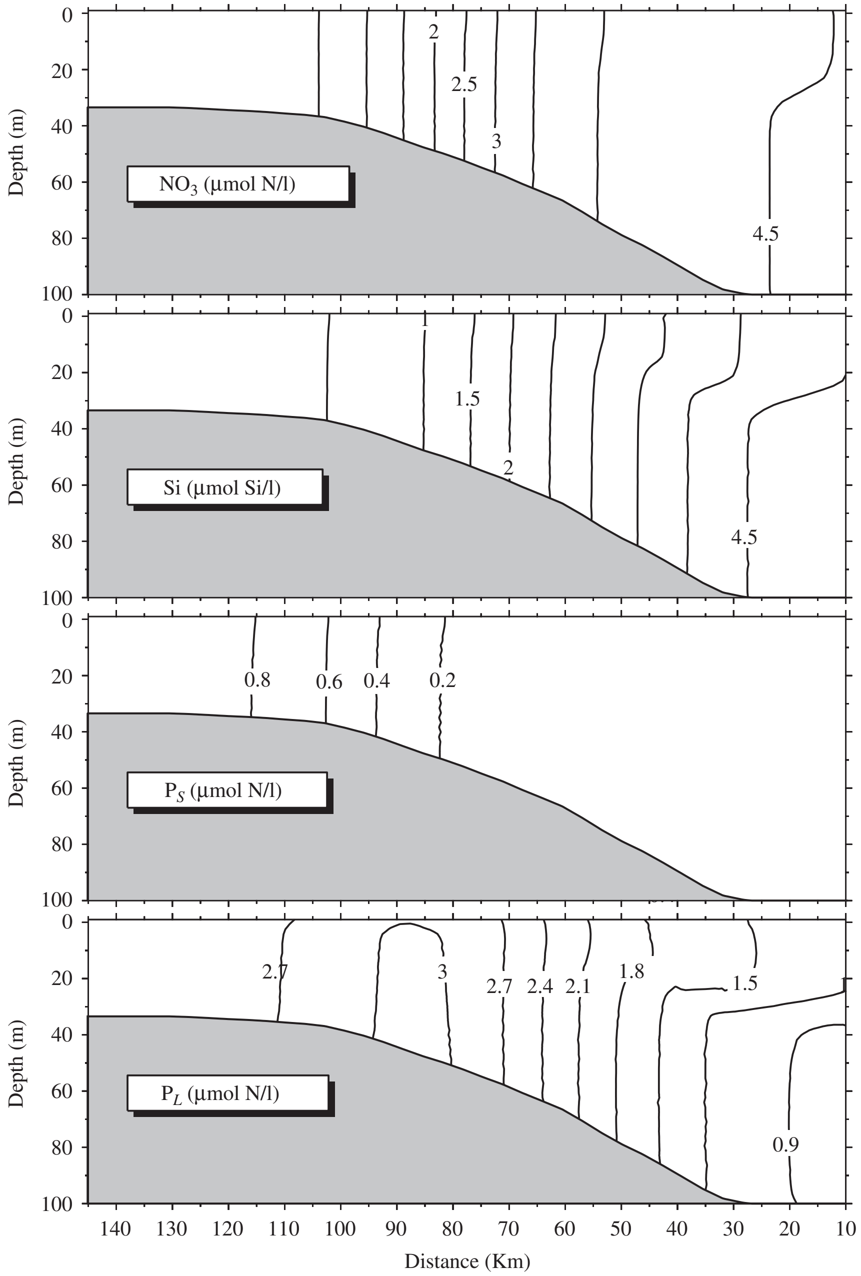

Fig. 10. Model-computed cross-isobath distribution of tidally averaged nitrate (NO_3), silicate (Si), small phytoplankton (P_S) and large phytoplankton (P_L) on the southern flank of GB on April 15, 1995.

continuous nutrient supply supports the relatively higher biomass of both small and large phytoplankton in this region as shown in the model results.

4.4. Comparison of model results with observations

One of the major issues of biological models is whether the model is capable of capturing the basic pattern of the system as understood from observational data. A direct comparison of the 1-D or 2-D model results with the observed data is difficult, mainly because those models cannot provide a realistic physical setting for the biological system due to simplified wind and tidal-forcing schemes, and more importantly, due to the lack of lateral advection processes for both biological and physical

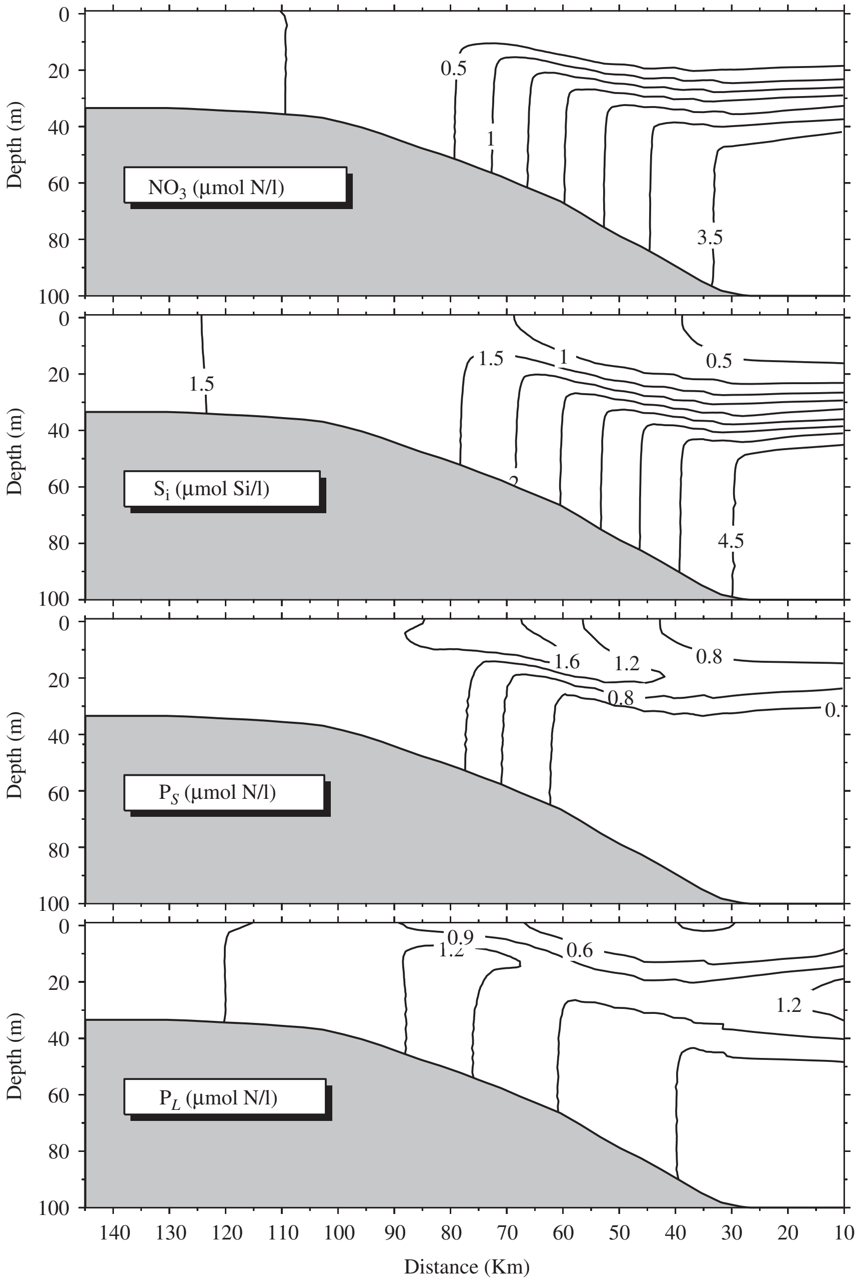

Fig. 11. Model-computed cross-isobath distribution of tidally averaged nitrate (NO_3), silicate (Si), small phytoplankton (P_S) and large phytoplankton (P_L) on the southern flank of GB on June 15, 1995.

quantities. Therefore, the comparison is qualitative and focuses more on the general patterns.

The 1-D model results at Site A were compared with data collected at Station 12 in 1999. This station represents a shallow mixing site on the top of the bank (67.542°W, 41.407°N), with water depth of about 41 m. A spring phytoplankton bloom in March and April with Chl-*a* concentration of ca. 6–7 µg/l was observed. The model results reproduced the bloom with good agreement of the timing and magnitude (Fig. 12, top panel). However, a relatively weaker bloom observed during June was not reproduced by the model, although the recovery of silicate concentration can be found both in

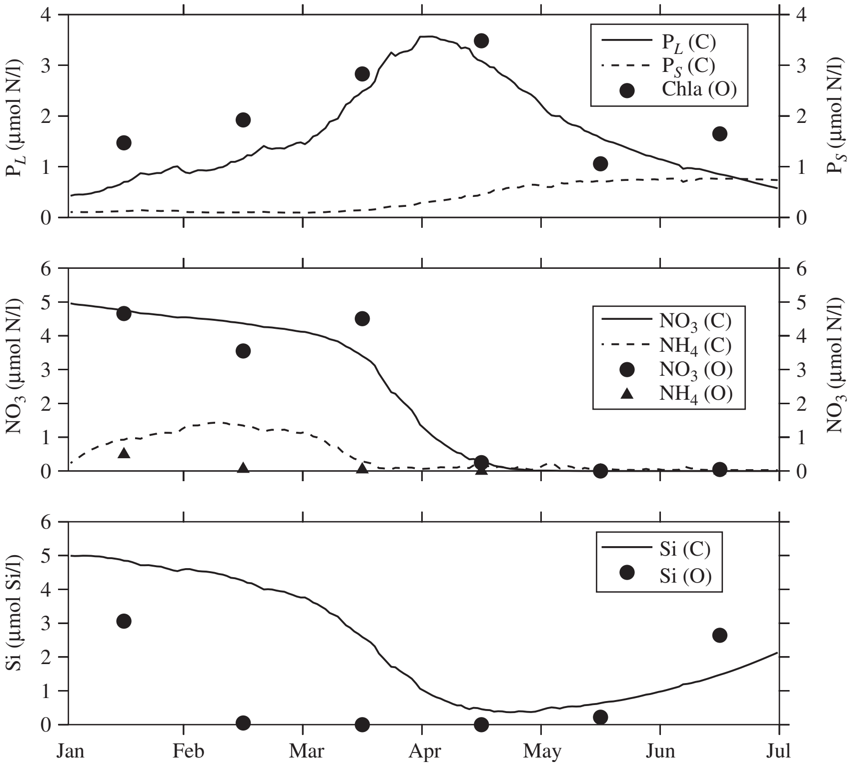

Fig. 12. Comparisons between the model-predicted and observed vertically averaged phytoplankton (top), nitrate (NO_3) (middle), ammonium (NH_4) (middle), and silicate (Si) (bottom) at Site A from January to June; (O): stands for observed value; (C): stands for computed value.

observation and the model (Fig. 12, bottom panel). The model was unable to explain the appearance of the "second" bloom (a diatom bloom occurred in later spring, Townsend and Thomas, 2002). From the point of view of nutrient dynamics in a 1-D domain, since nitrogen ($NO_3+NO_2+NH_4$) was very low as shown in both observation and model results (Fig. 12, middle panel). The internal recovery of silicate alone may not be able to trigger the "second" diatom bloom; the import of both nitrogen and silicate from the outside of the crest through tidal pumping and episodic strong wind events is likely to be another important nutrient source that fuels the long-lasting high phytoplankton concentration on the crest.

The 1-D model was much less successful at capturing the basic patterns of spring nutrient and phytoplankton dynamics in the surface layer at the deeper flank Site B as shown in comparisons to observations at Station 15 located at 66.700°W, 41.033°N. The model showed a strong bloom in the surface-mixing layer starting in mid-April and lasting for about 1 month, followed by a rapid decline. This bloom was even more significant than the one in the shallow mixing site, but with about a 1-month time lag (Fig. 13, top panel). The timing of this bloom appears to be related to the formation of weak stratification in mid-April. However, this bloom was not observed at stations along the flank area during both 1997 and 1999 (Townsend and Thomas, 2001, 2002). On the other hand, the model does not capture the weak bloom that was observed during March 1999, with Chl-$a > 3\,\mu g/l$. In addition, the observed depletion of silicate during March is almost 1 month earlier than in the model (Fig. 13, bottom panel). These significant differences between the model and observations in the deep site indicate that advection or other physical processes may play a significant role in the timing and magnitude of the springtime phytoplankton bloom on the flanks of GB. Due to the same reason, the 2-D model did not capture the right timing and magnitude of phytoplankton bloom in the deeper side of the model domain.

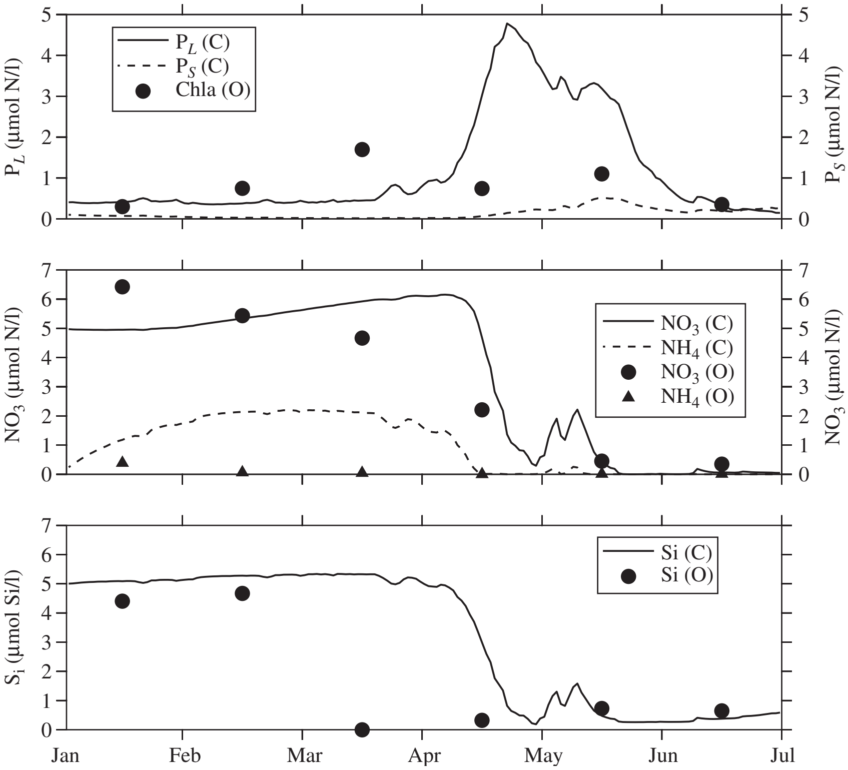

Fig. 13. Comparisons between the model-predicted and observed surface phytoplankton (top), nitrate (NO_3) (middle), ammonium (NH_4) (middle), and silicate (Si) (bottom) at Site B from January to June; (O): stands for observed value; (C): stands for computed value.

4.5. Model sensitivity analysis

A sensitivity analysis of the biological parameters is important to judge the reliability of the model. More importantly, it may indicate the necessity of improving the estimation of sensitive parameters. In this model, the sensitivity of biological parameters was estimated by

$$\hat{S} = \left| \frac{\Delta F/F}{\Delta \text{Parameter}/\text{Parameter}} \right|,$$

where $\hat{S}$ is the index of sensitivity, F is the concentration of a biological variable in the baseline model run with a standard set of biological parameters, and ΔF is the change of F caused by varying the model parameter. ΔParameter is the variation of the parameter in question by 1% from the baseline value. This method is the same as that used by Franks et al. (1986) and Fasham et al. (1990). According to the definition used in those previous studies, one parameter is considered to be sensitive when its sensitivity index $\hat{S} \geqslant 0.5$.

As an example, Fig. 14 shows that the diatom bloom (the large-sized phytoplankton concentration at the end of March in Fig. 12) is most sensitive to the ratio between nitrogen and silicon in diatoms (Rns). The temperature-dependent coefficient (Afa) for biological processes, including growth, mortality and grazing, is also a sensitive parameter. In addition, the loss terms of the diatoms, such as mortality (Epl) and grazing rate (Rzl) by large zooplankton are important. Overall, the spring bloom is significantly sensitive to only 2 of the 27 biological parameters in this model, suggesting that the results from this model are quantitatively meaningful.

The sensitivity of the phytoplankton bloom to physical forcings such as mixing and stratification was also examined for the deeper site in the 2-D model. This analysis tried to address the following two questions: (1) what strengths and durations of stratification will allow phytoplankton to bloom and show vertical structure, and (2) what is the response time of the phytoplankton to the development and decline of stratification? Fig. 15 (top two

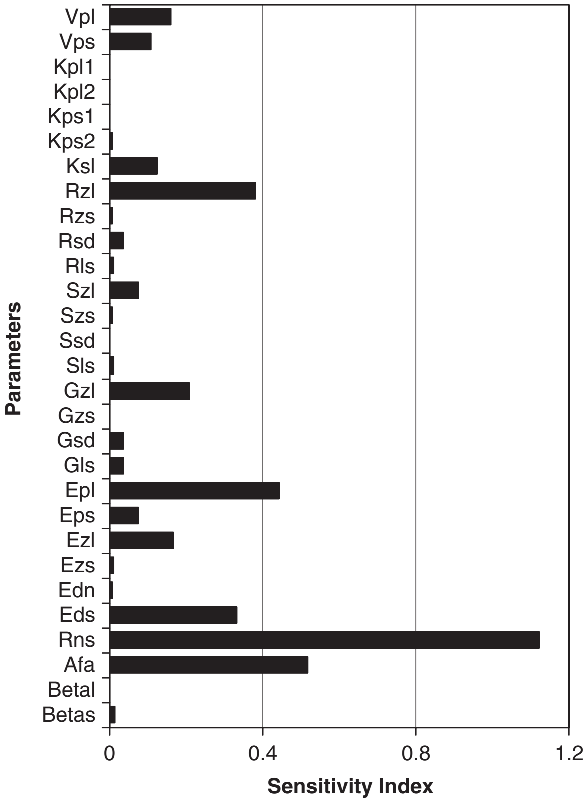

Fig. 14. Sensitivity of biological parameters in the model. The parameters listed on the *y*-axis are explained in Appendix A.2. The description of the computation of sensitivity index is given in Section 4.5.

panels) shows the temporal variation of the vertical temperature gradient ($\Delta T/\Delta Z$) and vertical eddy diffusivity (Km) in April. It can be seen that weak stratification with a temperature gradient (slightly higher than 0.02 °C/m) developed from April 25 to May 1 in the model. The positive growth of large phytoplankton occurred around April 20 and reached a peak value of $2.5\,\mu\mathrm{mol\,N\,l^{-1}}$ before the stratification broke down (Fig. 15, bottom panel), indicating that the spring bloom may be initiated as the vertical diffusion becomes weak (Townsend et al., 1992; Huisman et al., 1999). The responses of phytoplankton to the development of weak stratification were fairly quick, since the concentration almost doubled in 10 days from April 20 to 30, reaching $2.5\,\mu\mathrm{mol\,N\,l^{-1}}$. The decline of phytoplankton due to the breakdown of stratification was even faster, with a time scale of 1–2 day as a result of a moderate storm passing by during this period (shown in Fig. 2). Such a fluid condition also indicates that patches of phytoplankton can form and dissipate on small temporal and spatial scales, greatly complicating observations made with coarse spatial and temporal resolutions.

It is expected that the modeled stratification is sensitive to the variation of short-wave radiation. In model runs using 30% percent less short-wave radiation than the baseline model, the stratification was weaker (Fig. 16, top two panels). Consequently, the large phytoplankton bloom was much weaker, with a maximum concentration $<2.0\,\mu\mathrm{mol\,N\,l^{-1}}$. This result indicates that during the stratification transition time, biological processes are very sensitive to the surface heat flux. Realistic meteorological forcings are not only critical to the simulation of hydrodynamic fields, but also have significant influence on the biological system.

5. Discussion

5.1. The effect of light and nutrients on spring bloom

The spring phytoplankton bloom is usually a consequence of increasing light and nutrient supply and warmer temperature during the spring. Assuming the initial nutrient concentration is sufficient as the result of winter mixing processes, the light environment becomes critical to the timing of the spring bloom (Sverdrup, 1953). Observations on the southern flank of GB in 1995 (Beardsley et al., 2003) show that the maximum short-wave radiation strength increased from ca. $400\,\mathrm{W\,m^{-2}}$ in February to ca. $1000\,\mathrm{W\,m^{-2}}$ in June. The duration of daylight increased from ca. 10 h in February to 14 h in June, indicating an increasing incoming short-wave radiation and duration of photosynthesis through the modeled time period. The light attenuation coefficient K_{ext} is related to the varying components of total suspended solids, phytoplankton and dissolved organic matter. In this model, K_{ext} is computed as the sum of background light attenuation coefficient (K_0) and phytoplankton self-shading (K_s), where the value of K_0 might be affected by suspended sediment significantly. Therefore, a higher value of K_0 is expected on the shallow part of the bank during winter and early spring due to the high-suspended sediment concentration, caused by strong tide- and wind-induced mixing. In fact, when a higher K_0 value ($0.15\,\mathrm{m^{-1}}$) is used in the model, the spring bloom would occur about 2 months later than in the low K_0 ($0.1\,\mathrm{m^{-1}}$) case (results not shown). This is not a surprising result, yet it reminds us that the sensitivity of the bloom to the light

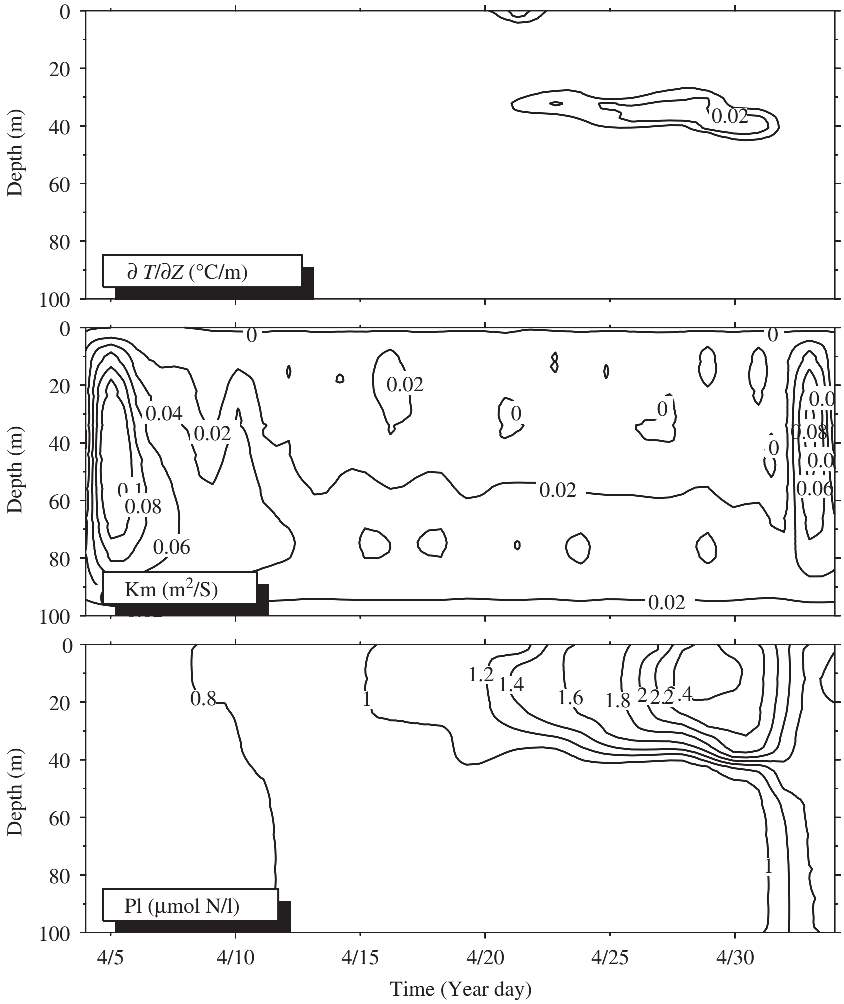

Fig. 15. Time sequence of the vertical distribution of model-predicted temperature gradient ($\Delta T/\Delta Z$), vertical turbulence mixing coefficient (K_m), and large phytoplankton (P_L) in the deep flank site.

environment is not negligible in this type of model. Since no sediment concentration was computed in the model, a simplified step-function (0.15 m^{-1} for January and February; 0.12 m^{-1} for March and April; 0.10 m^{-1} for May and June) were used for K_0 to reflect that the wind-induced sediment resuspension was more intense during early spring as shown in the time series data of surface wind stress in 1999 (Fig. 2). This parameterization appears to better capture the pattern of seasonal phytoplankton variation for the shallow model site (as shown in the baseline model results).

The results from the baseline 1-D model run indicate that silicate is depleted almost at the same time as nitrate during March. This pattern is different from the observations in which silicate was regarded as a limiting nutrient for phytoplankton as early as February. By adjusting the N/Si ratio of large phytoplankton, the modeled scenario of synchronized depletion of nitrate and silicate can be varied. If the N/Si ratio decreases to 0.8, meaning more silicate is needed per unit of nitrogen, silicate is depleted much earlier than the case with high N/Si ratio (Fig. 17). It is not surprising to see that a spring bloom is less likely to occur in this situation with a fixed half saturation constant due to the early limitation of silicate. In fact, as shown in the sensitivity analysis of all the biological parameters (Section 4.5), the N/Si ratio is the most sensitive biological parameter in terms of the diatom bloom in the model.

The failure of this model to reproduce significant spring blooms under early silicate depletion suggests that the silicate uptake and assimilation is more

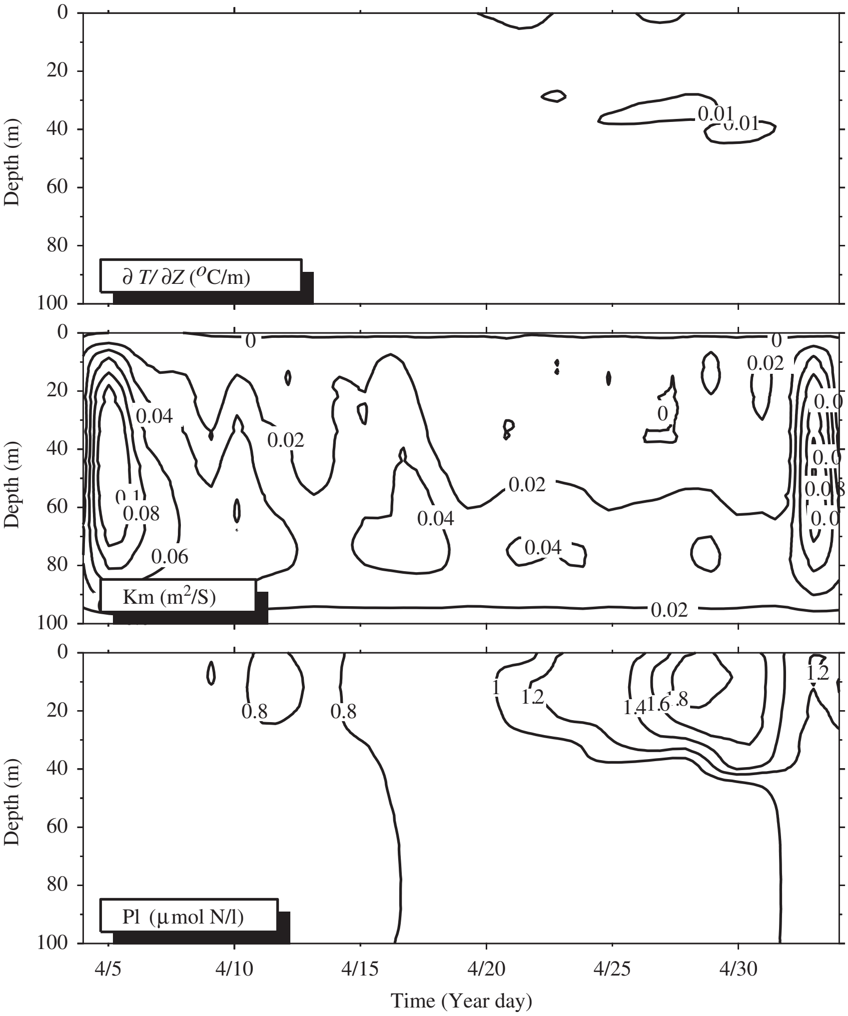

Fig. 16. Time sequence of the vertical distribution of model-predicted temperature gradient ($\Delta T/\Delta Z$), vertical turbulence mixing coefficient (K_m), and large phytoplankton (P_L) in the deep flank site with 30% less of surface heat flux.

complex than this model represents. It is necessary to be aware of the different roles of nitrogen and silica within the diatom cells. Nitrogen is a functional nutrient of the cell, a necessary constituent of the amino acids and proteins that mediate photosynthesis and cell growth. The growth rate will decrease under conditions of stress. In contrast, silica can be considered as a structural nutrient since it is primarily required by the diatom to synthesize its frustules. Metabolically active silica pools constitute only a few percent of total cell silica (Werner, 1977). When silicate availability is limited, cells may sacrifice some structural (cell wall) silica to meet metabolic needs (Paasch, 1973). To some extent, nitrogen uptake by large phytoplankton may be unaffected by silicate availability within the cell (Davidson and Gurney, 1999). These observations suggest that the N/Si ratio and half saturation constants in diatoms are not constant, a fact that greatly complicates the modeling efforts. To simplify the model, a high constant N/Si ratio was used in order to obtain a better simulation of the spring bloom. As a result, the silica did not show depletion during February in this model.

5.2. Transition between shallow and deep areas

In the 2-D model, the nutrients and plankton dynamics in the shallow and deep part of the cross-bank section mirrored the 1-D dynamics well.

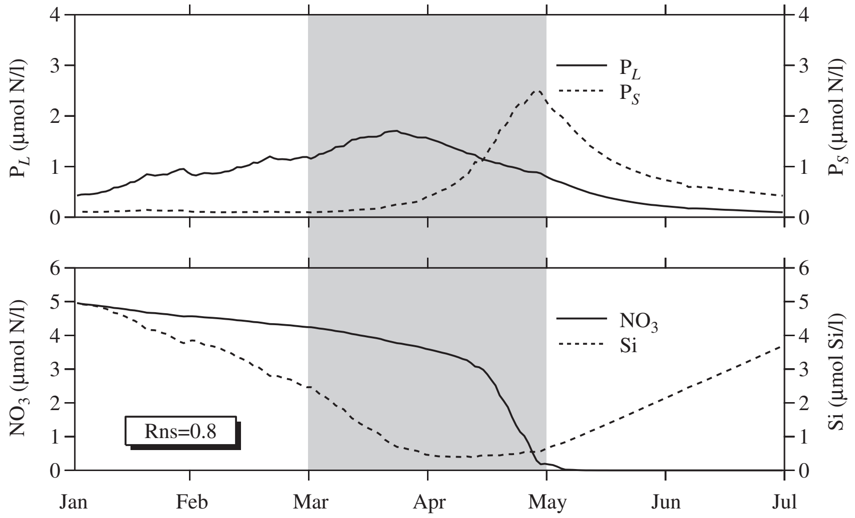

Fig. 17. Seasonal variation of large phytoplankton (P_L) and small phytoplankton (P_S) (top) when ratio of nitrogen and silicon (Rns) in large phytoplankton is 0.8. Bottom shows an asynchronous depletion of nitrate (NO_3) and silicate (Si), with silicate being depleted about 1 month earlier than nitrate.

The transition area in between, however, is unique in terms of the change of critical/mixing depth ratio and nutrient supply and consequently the phytoplankton dynamics.

As shown in the model results (Fig. 10), a narrow band of high phytoplankton concentration at 40–60 m water depth was observed during April. This area is coincident with the location of the later-developed tidal-mixing front during the stratified season, where a high concentration of phytoplankton has been detected from fluorescence measurement across the southern flank (Mountain and Taylor, 1996) At that time, however, no tidal-mixing front was seen in the model since the water was completely mixed even over the deep flank area. Therefore, the usual explanations for high phytoplankton concentration near a frontal area, such as water mass convergence and upfront transport of nutrients (Franks and Chen, 1996a) may not be applicable.

One possible explanation for the existence of a phytoplankton maximum area (PMA) in the model is the balance between light availability and nutrient supply from the deeper flank region. In the area shallower than 50 m, the biomass of phytoplankton starts to decline in April since nutrients are depleted by the end of spring bloom. However, the light intensity and day length during that time increased significantly, which deepens the critical depth. Meanwhile, in the deep flank area, no phytoplankton bloom occurred because the vertical mixing diluted the accumulation of phytoplankton biomass. As a result, a cross-bank nutrient gradient formed. During the flooding tide, high-nutrient water mixes with low-nutrient shallow water, causing a positive nutrient flux into waters near the 50-m isobath. This influx of nutrients supports phytoplankton growth, leading to a net increase of biomass (as the critical depth is less than the mixing depth). During ebb tide, some nutrients in the PMA have already been taken up by the phytoplankton; therefore, the loss of nutrients is less than the gain during flood time, causing a net influx of nutrients into the PMA.

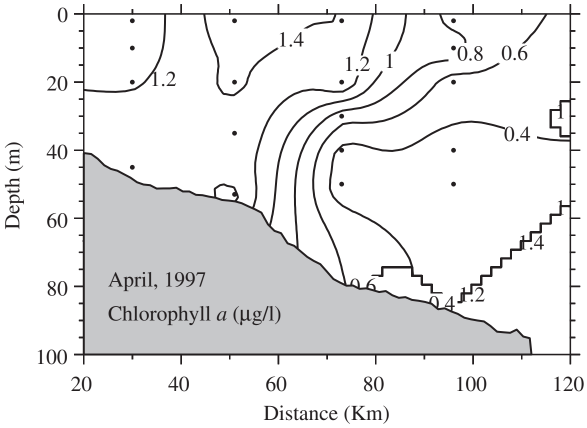

Fig. 18. An example of a phytoplankton maximum area (PMA) in the transition zone between shallow and deep areas along the cross-isobath section during April 1997.

The formation of the PMA is the consequence of the different timings of phytoplankton blooms and nutrient depletions in the shallow and deep regions, but this is just a model-predicted feature. Although, theoretically, the existence of the PMA is possible, it may be hard to observe in the field due to the complex topography and possible effects from lateral advective processes. Wind-induced cross-isobath advection may further complicate the situation. Fig. 18 shows a weak PMA in waters near the 50-m isobath from a transect across southern GB during April 1997 (observational data). It remains unclear whether such phenomena recur each year and are observable bank-wide. Further field measurements with better spatial resolution may be needed to validate this distribution pattern.

5.3. *Pros and cons of 1-D and 2-D models*

The 1-D model is probably a good start in order to distinguish the relative importance of local biological and physical processes by excluding the 3-D physical processes (e.g., upwelling and advection) (Hofmann and Ambler, 1988). In the shallow part of the bank, the spring bloom dynamics appear to be controlled primarily by local biological processes, whereas in the deep flank area, the local vertical stratification becomes more important as shown in the 1-D model results. The spring bloom dynamics on GB appears closely linked with not only local (including surface heating/cooling, tidal and wind mixing) but also remote physical processes, such as Scotian Shelf water inflow, advective transport from the interior of the GOM, low-salinity water over-across the Great South Channel (Butman et al., 1987; Beardsley et al., 1997; Chen et al., 2001), and on-bank intrusion of warm-core rings. However, implementing a fully 3-D model of such a complex system without understanding 1-D and 2-D dynamics will not only make the testing and verification of the 3-D model computationally costly, but also jeopardize the model's capability of identifying the roles played by individual biological and physical process.

2-D models have been applied to GB with various purposes, including the study of tidal mixing, internal wave generation, and cross-bank particle exchange (Chen et al., 1995a, b; Chen and Beardsley, 1998). More recently, the effects of wind and surface heating on the transport of water and particles through the tidal-mixing front on the southern flank of GB has been examined using a 2-D model (Chen et al., 2003a, b). Franks and Chen (1996a) coupled an NPZ model with a 2-D prognostic hydrodynamic model of a cross-bank section on GB to explore the influence of tidally generated mixing and advection on the development of patterns in the summertime plankton communities on GB and its surrounding fronts. All these modeling studies have been process studies simulating short time periods, usually less than a month. The basic assumption in these 2-D models is that no along-isobath variation exists, which is acceptable if the modeling time is relatively short. Due to the major circulation features of GB, it is not surprising to see that a 2-D model simulating 6 months will be less successful at capturing the basic biological patterns in the deep area than it will in the shallow central area. Therefore, similar to the 1-D case, caution must be taken to interpolate the 2-D model results, especially for the time after the onset of stratification in the deep side of the section.

Despite the limitations of our 1-D and 2-D models, the physical and biological factors controlling the spring bloom dynamics revealed in the 1-D and 2-D model studies can provide us with some insights on the inter-annual variability of nutrients, phytoplankton, zooplankton, and eventually the recruitment of commercially important fish species (cod and haddock) on the bank. It has been well recognized that there is a dynamic linkage between phytoplankton and target zooplankton species in the GOM/GB region (Wiebe et al., 2002). A phytoplankton-rich environment is critical to the growth and reproduction of *C. finmarchicus* and consequently the recruitment of cod and haddock as suggested by the "match and mismatch" theory (Cushing, 1975). The spring phytoplankton bloom usually occurs earlier in the shallow, well-mixed region as suggested by the 1-D/2-D models and observations. However, its contribution as a food source to the zooplankton population in the flank area is likely to be limited based on the 3-D tracer model experiments (Ji et al., 2006) except during some years when the "wash-out" of plankton from the central bank to the flank area occurs due to strong off-bank favorable wind events (Lewis et al., 2001). The mismatch between the 1-D/2-D model results and observations in the deep flank area suggests that the spring bloom dynamics is not only controlled by local biological (in situ growth) and physical (vertical stratification) processes in that area, but more likely influenced by advection, including water transport from the GOM, Scotian Shelf, and the slope. A better understanding of those processes and their impacts on the zooplankton and fish population dynamics require further extensive studies in a 3-D spatial domain as demonstrated by the companion paper in this volume (Ji et al., 2006).

6. Summary

The 1-D- and 2-D-coupled biological–physical models were built and tested based on observed features of lower trophic food web dynamics on GB. The biological model consists of nine compartments, including nutrients (nitrate, ammonium and silicate), phytoplankton (large and small size classes), zooplankton (large and small size classes), detrital organic nitrogen and detrital biogenic silica. The biological and physical factors controlling the timing and magnitude of spring bloom were examined using 1-D and 2-D modeling experiments driven by offshore tidal and observed meteorological surface forcing.

In the shallow and well-mixed central bank, the timing of the spring bloom is mainly controlled by the light environment (including light intensity and light attenuation coefficient), whereas in the relatively deeper flank area, the seasonally developing stratification controls the timing of the bloom. The bloom occurs earlier in the shallow-mixed site than that in the deep site. Correspondingly, the nutrients (nitrogen and silicate) are depleted earlier in the shallow site. The vertical gradients in the plankton and nutrient distributions at the deep site are caused by the phytoplankton bloom following the development of stratification after April.

Nitrogen appears to be the major limiting nutrient for phytoplankton growth. The contradiction between early depletion of silicate and months-long diatom blooms indicates the complex role of silica plays in the growth of diatoms. It is probably an over-simplification to use a constant (no temporal variation) N/Si ratio and half saturation constant of silicate uptake by diatoms in the model. The sensitivity analysis indicates that the model is most sensitive to the N/Si ratio of the diatoms with respect to the diatom bloom dynamics and the seasonal change of phytoplankton species composition.

The transition zone between the shallow and deep parts of the bank is caused by cross-isobath interaction of biological and physical processes. The model predicted a phytoplankton maximum area to occur between the shallow and deep areas prior to stratification as a result of light availability and continuous nutrient supply from deep, nutrient-rich waters through tidal-mixing processes. After stratification developed in the deep area, an area with an elevated phytoplankton concentration is observed in the model near the tidal-mixing front, which occurs as the result of nutrient supply from the deep water below the stratification layer.

Overall, the 1-D and 2-D modeling study identified the difference between central (well-mixed) and deep (seasonally stratified) areas of the bank in terms of timing and duration of spring bloom and associated lower trophic level food web dynamics. Understanding the system in 1-D and 2-D domains allows us to examine more complex biological and physical interactions in a fully 3-D model domain.

Acknowledgments

This research was supported by the US GLOBEC/GB IV Program through NSF Grants OCE0227679 and OCE0234545, NOAA Grant NA16OP2323, Georgia Sea Grant College Program NA06RG0029 to Changsheng Chen; a Woods Hole Oceanographic Institute Coastal Ocean Institute Postdoctoral Scholarship to Rubao Ji; NSF Grant OCE02-20111 to Peter Franks and Edward Durbin; NSF Grant OCE0227679 to Robert Beardsley; NSF Grant OCE-0236270 to Robert Houghton, David Townsend and Gregory Lough. We want to thank Qichun Xu, Geoff Cowles, Song Hu and Hedong Liu for their help with the setup of the GoM/GB hydrodynamics model. The comments of three anonymous reviewers are gratefully acknowledged. Special thanks go to Brian Binder (University of Georgia) and Cabell Davis (WHOI) for their help on the manuscripts and their continuing support. The US GLOBEC contribution number is 302, Lamont-Doherty Earth Observatory contribution number is 6931.

Appendix A. The biological model

A.1. Model equations

The lower trophic level food web model developed in this paper is a nine-compartment nutrients–phytoplankton–zooplankton–detritus (NPZD) model.

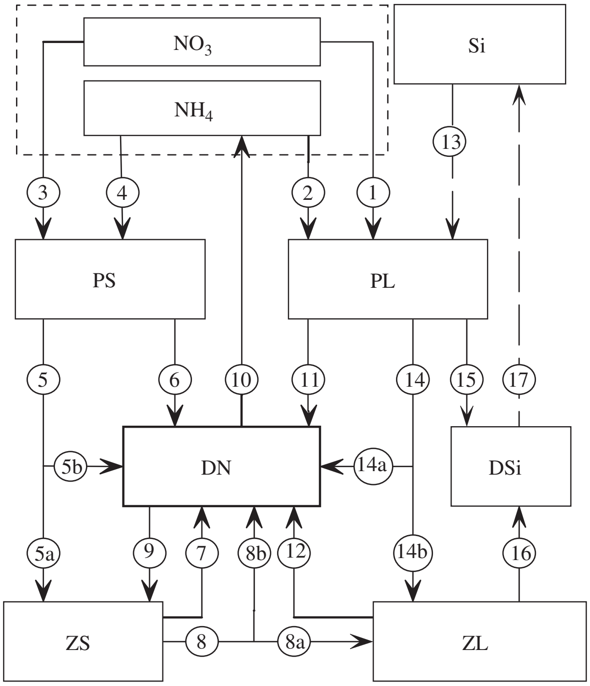

Fig. 19. Schematic of biological model with each process numbered. This figure represents the same model configuration as shown in Fig. 4, with numbered arrows indicating internal fluxes for the convenience of mathematical description of the biological source/sink terms given in the Appendix A.

The governing equations of this nine-compartment model are given as

$$\frac{\partial B}{\partial t} - \frac{\partial}{\partial z}\left(A_h \frac{\partial B}{\partial z}\right) = F_B,$$

where $B = (\mathrm{P_S}, \mathrm{P_L}, \mathrm{Z_S}, \mathrm{Z_L}, \mathrm{NO_3}, \mathrm{NH_4}, \mathrm{D_N}, \mathrm{Si}, \mathrm{D_{Si}})$ with $\mathrm{P_S}$: small-phytoplankton biomass (μmol N l^{-1}); $\mathrm{P_L}$: large-phytoplankton biomass (μmol N l^{-1}); $\mathrm{Z_S}$: small-zooplankton biomass (μmol N l^{-1}); $\mathrm{Z_L}$: large-zooplankton biomass (μmol N l^{-1}); NO$_3$: nitrate concentration (μmol N l^{-1}), NH$_4$: ammonium concentration (μmol N l^{-1}); $\mathrm{D_N}$: particulate organic nitrogen concentration (μmol N l^{-1}); Si: silicate concentration (μmolSi l^{-1}); $\mathrm{D_{Si}}$: particulate biogenic silica concentration (μmolSi l^{-1}). A_h is the thermal diffusion coefficient that is calculated using the Mellor and Yamada level 2.5 turbulent closure scheme incorporated in the physical model.

On the right-hand side of the above equation, F_B is computed by adding incoming flux and subtracting outgoing flux shown in Fig. 19, where each number indicates an internal flux defined as following:

f1/f3: uptake of nitrate by large/small phytoplankton (μmol N l^{-1}day^{-1});
f2/f4: uptake of ammonium by large/small phytoplankton (μmol N l^{-1} day^{-1});
f5: small zooplankton grazing on small phytoplankton (μmol N l^{-1} day^{-1});
f5a: assimilated part of f5 (μmol N l^{-1} day^{-1});
f5b: un-assimilated part of f5 (μmol N l^{-1}day^{-1});
f6/f7: mortality of small/large phytoplankton (μmol N l^{-1}day^{-1});
f8: large zooplankton grazing on small zooplankton (μmol N l^{-1} day^{-1});
f8a: assimilated part of f8 (μmol N l^{-1} day^{-1});
f8b: un-assimilated part of f8 (μmol N l^{-1} day^{-1});
f9: small zooplankton grazing on detritus nitrogen (μmol N l^{-1}day^{-1});
f10: remineralization of particulate organic nitrogen (μmol N l^{-1}day^{-1});
f11: mortality of large phytoplankton (in term of N) (μmol N l^{-1} day^{-1});
f12: mortality of large zooplankton (μmol N l^{-1} day^{-1});
f13: uptake of silicate by large phytoplankton (μmol Si l^{-1} day^{-1});
f14: large zooplankton grazing on large phytoplankton (μmol N l^{-1} day^{-1});
f14a: assimilated part of f14 (μmol N l^{-1} day^{-1});
f14b: un-assimilated part of f14 (μmol N l^{-1} day^{-1});
f15: mortality of large phytoplankton (in term of Si) (μmol Si l^{-1}day^{-1});
f16: silica rejected from large zooplankton (μmol Si l^{-1} day^{-1});
f17: dissolution of particulate organic silica (μmol Si l^{-1} day^{-1}).

$$f1 = \frac{L^{\mathrm{P_L}}_{\mathrm{NH_4}}}{L^{\mathrm{P_L}}_{\mathrm{NO_3}} + L^{\mathrm{P_L}}_{\mathrm{NH_4}}} \min\left\{\left(L^{\mathrm{P_L}}_{\mathrm{NO_3}} + L^{\mathrm{P_L}}_{\mathrm{NH_4}}\right), L^{\mathrm{P_L}}_{\mathrm{Si}}\right\} \times V^{\mathrm{P_L}}_{\max} L^{\mathrm{P_L}}_{I} \mathrm{P_L},$$

$$f2 = \frac{L^{\mathrm{P_L}}_{\mathrm{NO_3}}}{L^{\mathrm{P_L}}_{\mathrm{NO_3}} + L^{\mathrm{P_L}}_{\mathrm{NH_4}}} \min\left\{\left(L^{\mathrm{P_L}}_{\mathrm{NO_3}} + L^{\mathrm{P_L}}_{\mathrm{NH_4}}\right), L^{\mathrm{P_L}}_{\mathrm{Si}}\right\} \times V^{\mathrm{P_L}}_{\max} L^{\mathrm{P_L}}_{I} \mathrm{P_L},$$

$$L^{\mathrm{P_L}}_{\mathrm{NO_3}} = \frac{\mathrm{NO_3}}{k^{\mathrm{P_L}}_{\mathrm{NO_3}} + \mathrm{NO_3}} \frac{1}{1 + \left(\mathrm{NH_4}/\beta_{\mathrm{P_L}}\right)},$$

$$L_{\mathrm{NH_4}}^{\mathrm{P_L}} = \frac{\mathrm{NH_4}}{k_{\mathrm{NH_4}}^{\mathrm{P_L}} + \mathrm{NH_4}},$$

$$f3 = V_{\max}^{\mathrm{P_S}} L_{\mathrm{NO_3}}^{\mathrm{P_S}} L_I^{\mathrm{P_S}} \mathrm{P_S},$$

$$f4 = V_{\max}^{\mathrm{P_S}} L_{\mathrm{NH_4}}^{\mathrm{P_S}} L_I^{\mathrm{P_S}} \mathrm{P_S},$$

$$L_{\mathrm{NO_3}}^{\mathrm{P_S}} = \frac{\mathrm{NO_3}}{k_{\mathrm{NO_3}}^{\mathrm{P_S}} + \mathrm{NO_3}} \frac{1}{1 + \left(\mathrm{NH_4}/\beta_{\mathrm{P_S}}\right)},$$

$$L_{\mathrm{NH_4}}^{\mathrm{P_S}} = \frac{\mathrm{NH_4}}{k_{\mathrm{NH_4}}^{\mathrm{P_S}} + \mathrm{NH_4}},$$

$$f5 = G_{\max}^{\mathrm{Z_S}} \left(1 - \mathrm{e}^{\left(-k^{\mathrm{P_S}} \mathrm{P_S}\right)}\right) \mathrm{Z_S},$$

$$f5\mathrm{a} = \varepsilon^{\mathrm{Z_S}} f5,$$

$$f5\mathrm{b} = (1 - \varepsilon^{\mathrm{Z_S}}) f5,$$

$$f6 = \alpha^{\mathrm{P_S}} \mathrm{P_S},$$

$$f7 = \alpha^{\mathrm{Z_S}} \mathrm{Z_S^2},$$

$$f8 = G_{\max}^{Z_{\mathrm{LS}}} \left(1 - \mathrm{e}^{\left(-k_{\mathrm{LS}}^{Z} \mathrm{Z_S}\right)}\right) \mathrm{Z_L},$$

$$f8\mathrm{a} = \varepsilon^{\mathrm{Z_{LS}}} f8,$$

$$f8\mathrm{b} = \left(1 - \varepsilon^{\mathrm{Z_{LS}}}\right) f8,$$

$$f9 = G_{\max}^{Z_{\mathrm{SD}}} \left(1 - \mathrm{e}^{\left(-k^{Z_{\mathrm{SD}}} \mathrm{D_N}\right)}\right) \mathrm{Z_S},$$

$$f10 = e_{\mathrm{N}} \mathrm{D_N},$$

$$f11 = \alpha^{\mathrm{P_L}} \mathrm{P_L},$$

$$f12 = \alpha^{\mathrm{Z_L}} \mathrm{Z_L^2},$$

$$f13 = \lambda_{\mathrm{SIN}}^{P_{\mathrm{L}}} (f1 + f2),$$

$$f13 = \lambda_{\mathrm{SIN}}^{P_{\mathrm{L}}} (f1 + f2),$$

$$f14 = G_{\max}^{\mathrm{Z_L}} \left(1 - \mathrm{e}^{\left(-k^{\mathrm{P_L}} \mathrm{P_L}\right)}\right) \mathrm{Z_L},$$

$$f14\mathrm{a} = \varepsilon^{\mathrm{Z_L}} f14,$$

$$f14\mathrm{b} = (1 - \varepsilon^{\mathrm{Z_L}}) f14,$$

$$f15 = \lambda_{\mathrm{SEN}}^{\mathrm{P_L}} f11,$$

$$f16 = \lambda_{\mathrm{SEN}}^{\mathrm{P_L}} f14,$$

$$f17 = e_{\mathrm{Si}} \mathrm{D_{Si}}.$$

A.2. Model parameters

Parameters	Definition	Value
$V_{\max}^{\mathrm{P_L}}$ (Vpl)	Maximum growth rate for $\mathrm{P_L}$	3.0 day^{-1}
$V_{\max}^{\mathrm{P_S}}$ (Vps)	Maximum growth rate for $\mathrm{P_S}$	2.4 day^{-1}
$k_{\mathrm{NO_3}}^{\mathrm{P_L}}$ (Kpl1)	Half-saturation constant for $\mathrm{NO_3}$ uptake by $\mathrm{P_L}$	1.0 μmol N l^{-1}
$k_{\mathrm{NH_4}}^{\mathrm{P_L}}$ (Kpl2)	Half-saturation constant for $\mathrm{NH_4}$ uptake by $\mathrm{P_L}$	0.2 μmol N l^{-1}
$k_{\mathrm{NO_3}}^{\mathrm{P_S}}$ (Kps1)	Half-saturation constant for $\mathrm{NO_3}$ uptake by $\mathrm{P_S}$	0.5 μmol N l^{-1}
$k_{\mathrm{NH_4}}^{\mathrm{P_S}}$ (Kps2)	Half-saturation constant for $\mathrm{NH_4}$ uptake by $\mathrm{P_S}$	0.05 μmol N l^{-1}
$k_{\mathrm{Si}}^{\mathrm{P_L}}$ (Ksl)	Half-saturation constant for Si uptake by $\mathrm{P_L}$	2.0 μmol Si l^{-1}
$G_{\max}^{\mathrm{Z_L}}$ (Rzl)	Maximum grazing rate of $\mathrm{Z_L}$ on $\mathrm{P_L}$	0.3 day^{-1}
$G_{\max}^{\mathrm{Z_S}}$ (Rzs)	Maximum grazing rate of $\mathrm{Z_S}$ on $\mathrm{P_S}$	0.5 day^{-1}
$G_{\max}^{Z_{\mathrm{LS}}}$ (Rls)	Maximum grazing rate of $\mathrm{Z_L}$ on $\mathrm{Z_S}$	0.3 day^{-1}
$G_{\max}^{Z_{\mathrm{SD}}}$ (Rsd)	Maximum grazing rate of $\mathrm{Z_S}$ on $\mathrm{D_N}$	0.5 day^{-1}
$k^{\mathrm{P_L}}$ (Szl)	Ivlev constant for $\mathrm{Z_L}$ grazing on $\mathrm{P_L}$	1.0 μmol N l^{-1}
$k^{\mathrm{P_S}}$ (Szs)	Ivlev constant for $\mathrm{Z_S}$ grazing on $\mathrm{P_S}$	0.5 μmol N l^{-1}

$k^{Z_{SD}}$ (Ssd)	Ivlev constant for Z_S grazing on D_N	$1.0\,\mu\mathrm{mol\,N\,l}^{-1}$
$k^{Z_{LS}}$ (Sls)	Ivlev constant for Z_L grazing on Z_S	$1.0\,\mathrm{l}\,\mu\mathrm{mol}^{-1}\,\mathrm{N}^{-1}$
ε^{Z_L} (Gzl)	Assimilation efficiency of Z_L grazing on P_L	0.35
ε^{Z_S} (Gzs)	Assimilation efficiency of Z_S grazing on P_S	0.4
$\varepsilon^{Z_{SD}}$ (Gsd)	Assimilation efficiency of Zs grazing on D_N	0.2
$\varepsilon^{Z_{LS}}$ (Gls)	Assimilation efficiency of Z_L on Z_S	0.4
α^{P_L} (Epl)	Mortality rate of P_L	$0.1\,\mathrm{day}^{-1}$
α^{P_S} (Eps)	Mortality rate of P_S	$0.2\,\mathrm{day}^{-1}$
α^{Z_L} (Ezl)	Mortality rate of Z_L	$0.2\,\mathrm{day}^{-1}$
α^{Z_S} (Ezs)	Mortality rate of Z_S	$0.2\,\mathrm{day}^{-1}$
e_{D_N} (Edn)	Remineralization rate of D_N	$0.05\,\mathrm{day}^{-1}$
$e_{D_{Si}}$ (Eds)	Dissolution rate of D_{si}	$0.03\,\mathrm{day}^{-1}$
$\lambda^{P_L}_{Si:N}$ (Rns)	Ratio of Si versus N in P_L	0.67
α (Afa)	Temperature dependent coefficient	2.0
β_{P_L} (Betal)	NH_4 inhibition on NO_3 uptake for P_L	$0.4\,\mu\mathrm{mol\,N\,l}^{-1}$
β_{P_S} (Betas)	NH_4 inhibition on NO_3 uptake for P_S	$0.2\,\mu\mathrm{mol\,N\,l}^{-1}$

A.3. Boundary conditions

The surface and bottom boundary conditions for biological variables are specified as

$$\frac{\partial}{\partial z}(Z_S, Z_L, \mathrm{NO_3}, \mathrm{NH_4}, \mathrm{Si}) = 0 \quad \text{at}\, z = \zeta, -H,$$

$$\frac{\partial P_L}{\partial z} = \frac{w_{P_L}}{A_h} P_L; \quad \frac{\partial P_s}{\partial z} = \frac{w_{P_S}}{A_h} P_S; \quad \text{at}\, z = \zeta, -H,$$

$$\frac{\partial D_N}{\partial z} = \frac{w_{D_N}}{A_h} D_N; \quad \frac{\partial D_{Si}}{\partial z} = \frac{w_{D_{Si}}}{A_h} D_{Si}; \quad \text{at}\, z = \zeta, -H,$$

where $w_{P_L}, w_{P_S}, w_{D_N}$ and $w_{D_{Si}}$ are the sinking velocities of P_L, P_S, D_N, and D_{Si}, respectively.

References

Beardsley, R.C., Butman, B., Geyer, W.R., Smith, P., 1997. Physical oceanography of the Gulf of Maine: an update. Proceedings of the Gulf of Maine Ecosystem Dynamics Scientific Symposium and Workshop. Regional Association for Research in the Gulf of Maine, Hanover NH, USA, pp. 39–52.

Beardsley, R.C., Lentz, S.J., Weller, R.A., Limeburner, R., Irish, J.D., Edson, J.B., 2003. Surface forcing on the southern flank of Georges Bank, February–August 1995. Journal of Geophysical Research-Oceans 108, 8007.

Blumberg, A.F., 1994. A primer for ECOM3D-si. Technical Report. HydroQual, Inc., Mahwah, NJ, 84pp.

Brzezinski, M.A., 1985. The silicon:carbon:nitrogen ratio of marine diatoms: interspecific variability and the effect of some environmental variables. Journal of Phycology 21, 347–357.

Butman, B., Loder, J.W., Beardsley, R.C., 1987. The seasonal mean circulation: observation and theory. In: Backus, R.H., Bourne, D.W. (Eds.), Georges Bank. MIT Press, Cambridge, MA, pp. 125–138.

Chen, C., Beardsley, R., 1998. Tidal mixing and cross-frontal particle exchange over a finite amplitude asymmetric bank: a model study with application to Georges Bank. Journal of Marine Research 56, 1163–1201.

Chen, C., Beardsley, R., 2002. Cross-frontal water exchange on Georges Bank: modeling exploration of the US GLOBEC/Georges Bank phase III study. Journal of Oceanography 58, 403–420.

Chen, C., Beardsley, R.C., Limeburner, R., 1995a. Numerical study of stratified tidal rectification over finite-amplitude banks. Part II: Georges Bank. Journal of Physical Oceanography 25, 2111–2128.

Chen, C., Beardsley, R.C., Limeburner, R., 1995b. Variability of water properties in late spring in the northern Great South Channel. Continental Shelf Research 15, 415–431.

Chen, C., Beardsley, R.C., Franks, P.J.S., 2001. A 3-D prognostic model study of the ecosystem over Georges Bank and adjacent coastal regions. Part I: physical model. Deep-Sea Research II 48, 419–456.

Chen, C., Ji, R., Schwab, D.J., Beletsky, D., Fahnenstiel, G.L., Jiang, M., Johengen, T.H., Vanderploeg, H., Eadie, B., Budd, J.W., Bundy, M.H., Gardner, W., Cotner, J., Lavrentyev, P.J., 2002. A model study of the coupled biological and physical dynamics in Lake Michigan. Ecological Modelling 152, 145–168.

Chen, C.S., Beardsley, R.C., Franks, P.J.S., Van Keuren, J., 2003a. Influence of diurnal heating on stratification and residual circulation of Georges Bank. Journal of Geophysical Research-Oceans 108, 8008.

Chen, C.S., Schlitz, R.J., Lough, R.G., Smith, K.W., Beardsley, R., Manning, J.P., 2003b. Wind-induced, cross-frontal exchange on Georges Bank: a mechanism for early summer on-bank biological particle transport. Journal of Geophysical Research-Oceans 108, 8011.

Chen, C., Beardsley, R., Hu, S., Xu, Q., Liu, H., 2005. Using MM5 to Hindcast the ocean surface forcing fields over the Gulf of Maine and Georges Bank Region. Journal of Atmospheric and Oceanic Technology 22, 131–145.

Cura, J.J., 1987. Phytoplankton. In: Backus, R.H., Bourne, D.W. (Eds.), Georges Bank. MIT Press, Cambridge, MA, pp. 213–218.

Cushing, D.H., 1975. Marine Ecology and Fisheries. Cambridge University Press, London, pp. 1–277.

Davidson, K., Gurney, W.S.C., 1999. An investigation of non-steady-state algal growth. II. Mathematical modeling of co-nutrient-limited algal growth. Journal of Plankton Research 21, 839–858.

Davis, C.S., 1987. Zooplankton life cycles. In: Backus, R.H., Bourne, D.W. (Eds.), Georges Bank. MIT Press, Cambridge, MA, pp. 256–267.

Denman, K.L., Gargett, A.E., 1995. Biological physical interactions in the upper ocean—the role of vertical and small-scale transport processes. Annual Review of Fluid Mechanics 27, 225–255.

Druffel, E.R.M., Williams, P.M., Bauer, J.E., Ertel, J.R., 1992. Cycling of dissolved and particulate organic matter in the open Oceanography. Journal of Geophysical Research 97, 15639–15659.

Eilers, P.H.C., Peeters, J.C.H., 1988. A model for the relationship between light intensity and the rate of photosynthesis in phytoplankton. Ecological Modelling 42, 199–215.

Eslinger, D.L., Iverson, R.L., 2001. The effects of convective and wind-driven mixing on spring phytoplankton dynamics in the Southeastern Bering Sea middle shelf domain. Continental Shelf Research 21, 627–650.

Eslinger, D.L., Cooney, R.T., Mcroy, C.P., Ward, A., Kline, T.C., Simpson, E.P., Wang, J., Allen, J.R., 2001. Plankton dynamics: observed and modelled responses to physical conditions in Prince William Sound, Alaska. Fisheries Oceanography 10, 81–96.

Falkowski, P.G., Wirick, C.D., 1981. A simulation model of the effects of vertical mixing on primary productivity. Marine Biology 65, 69–75.

Fasham, M.J.R., 1995. Variations in the seasonal cycle of biological production in subarctic oceans: a model sensitivity analysis. Deep-Sea Research I 42, 1111–1149.

Fasham, M.J.R., Duklow, H.W., McKelvie, S.M., 1990. A nitrogen-based model of plankton dynamics in the oceanic mixed layer. Journal of Marine Research 48, 591–639.

Franks, P.J.S., Chen, C., 1996a. Plankton production in tidal fronts: a model of Georges Bank in summer. Journal of Marine Research 54, 631–651.

Franks, P.J.S., Chen, C.S., 1996b. Plankton production in tidal fronts: a model of Georges Bank in summer. Journal of Marine Research 54, 631–651.

Franks, P.J.S., Chen, C., 2001. A 3-D prognostic numerical model study of the Georges Bank ecosystem. Part II: biological-physical model. Deep-Sea Research II 48, 457–482.

Franks, P.J.S., Wroblewski, J.S., Flierl, G.R., 1986. Behavior of a simple plankton model with food-level acclimation by herbivors. Marine Biology 91, 121–129.

Frost, B.W., Franzen, N.C., 1992. Grazing and iron limitation in the control of phytoplankton stock and nutrient concentration: a chemostat analog of the Pacific equatorial upwelling zone. Marine Ecology Progress Series 83, 291–303.

Gallegos, C.L., Vant, W.N., 1996. An incubation procedure for estimating carbon-to-chlorophyll ratios and growth irradiance relationships of estuarine phytoplankton. Marine Ecology Progress Series 138, 275–291.

Garrett, C.J.R., Loder, J.W., 1981. Dynamical aspects of shallow sea fronts. Philosophical Transactions of the Royal Society of London A 302, 563–581.

Hofmann, E.E., Ambler, J.W., 1988. Plankton dynamics on the outer Southeastern United-States Continental-Shelf: 2. A time-dependent biological model. Journal of Marine Research 46, 883–917.

Huisman, J., van Oostveen, P., Weissing, F.J., 1999. Critical depth and critical turbulence: two different mechanisms for the development of phytoplankton blooms. Limnology and Oceanography 44, 1781–1787.

Ivlev, V.S., 1961. Experimental Ecology of the Feeding of Fishes. Yale University Press, New Haven, CT.

Janowitz, G.S., Kamykowski, D., 1991. An Eulerian model of phytoplankton photosynthetic response in the upper mixed layer. Journal of Plankton Research 13, 988–1002.

Jassby, A.D., Platt, T., 1976. Mathematical formulation of the relationship between photosynthesis and light for phytoplankton. Limnology and Oceanography 21, 540–547.

Ji, R., Chen, C., Budd, J.W., Schwab, D.J., Beletsky, D., Fahnenstiel, G.L., Johengen, T.H., Vanderploeg, H., Eadie, B., Bundy, M., Gardner, W., Cotner, J., 2002. Influences of suspended sediments on the ecosystem in Lake Michigan: a 3-D coupled bio-physical modeling experiment. Ecological Modelling 152, 169–190.

Ji, R., Chen, C., Franks, P.J.S., Townsend, D.W., Durbin, A.G., Beardsley, R., Lough, R.G., Houghton, R.W., 2006. The impact of Scotian Shelf Water "cross-over" on the plankton dynamics on Georges Bank: a 3-D experiment for the 1999 spring bloom. Deep-Sea Research II, this issue [doi:10.1016/j.dsr2.2006.08.007].

Klein, P., 1987. A simulation of some physical and biological interactions. In: Backus, R.H., Bourne, D.W. (Eds.), Georges Bank. MIT Press, Cambridge, MA, pp. 395–402.

Lacroix, G., Nival, P., 1998. Influence of meteorological variability on primary production dynamics in the Ligurian Sea (NW Mediterranean Sea) with a 1D hydrodynamic/biological model. Journal of Marine Systems 16, 23–50.

Lewis, C.V., Davis, C.S., Gawarkiewicz, G., 1994. Wind-forced biological-physical interactions on an isolated off-shore bank. Deep-Sea Research II 41, 51–73.

Lewis, C.V.W., Chen, C., Davis, C.S., 2001. Effect of winter wind variability on plankton transport over Georges Bank. Deep-Sea Research II 48, 137–158.

Mellor, G.L., Yamada, T., 1982. Development of a turbulence closure model for geophysical fluid problems. Reviews of Geophysics and Space Physics 20, 851–875.

Mergard, R.O., Tonkyo, D.W., Senft, W.H., 1984. Kinetics of oxygenic photosynthesis in planktonic algae. Journal of Plankton Research 6, 325–337.

Mountain, D.G., Taylor, M.H., 1996. Fluorescence structure in the region of the tidal mixing front on the southern flank of Georges Bank. Deep-Sea Research II 43, 1831–1853.

O'Reilly, J.E., Evans-Zetlin, C.E., Busch, D.A., 1987. Primary production. In: Backus, R.H., Bourne, D.W. (Eds.), Georges Bank. MIT Press, Cambridge, MA, pp. 220–233.

Ohman, M.D., Hirche, H.J., 2001. Density-dependent mortality in an oceanic copepod population. Nature 412, 638–641.

Paasch, E., 1973. Silicon and the ecology of marine plankton diatoms. II. Silicate uptake kinetics in five diatoms species. Marine Biology 19, 262–269.

Pahl-Wostl, C., Imboden, D.M., 1990. DYPHORA—a dynamic model for the rate of photosynthesis of algae. Journal of Plankton Research 12, 1207–1221.

Parsons, T.R., Takahashi, M., Hargrave, B., 1984. Biological Oceanographic Processes. Pergamon Press, New York.

Platt, T., Gallegos, C.L., Harrison, W.G., 1980. Photoinhibition of photosynthesis in natural assemblages of marine phytoplankton. Journal of Marine Research 38, 687–701.

Reynolds, C.S., 1984. The Ecology of Freshwater Phytoplankton. Cambridge University Press, Cambridge, MA.

Scavia, D., Lang, G.A., Kitchell, J.F., 1988. Dynamics of Lake Michigan plankton: a model evaluation of nutrient loading, competition, and predation. Canadian Journal of Fisheries and Aquatic Sciences 45, 165–177.

Steele, J.H., 1962. Environmental control of photosynthesis in the sea. Limnology and Oceanography 7, 137–150.

Steele, J.H., Henderson, E.W., 1992. The role of predation in plankton models. Journal of Plankton Research 14, 157–172.

Strickland, J.D.H., 1960. Measuring the production of marine phytoplankton. Bulletin of the Fisheries Research Board of Canada 122, 1–172.

Sverdrup, H.U., 1953. On conditions for the vernal blooming of phytoplankton. Journal du Conseil International pour l'Exploration de la Mer 18, 287–295.

Thomas, A.C., Townsend, D.W., Weatherbee, R., 2003. Satellite-measured phytoplankton variability in the Gulf of Maine. Continental Shelf Research 23, 971–989.

Townsend, D.W., Thomas, A.C., 2001. Winter–spring transition of phytoplankton chlorophyll and inorganic nutrients on Georges Bank. Deep-Sea Research II—Topical Studies in Oceanography 48, 199–214.

Townsend, D.W., Thomas, M., 2002. Springtime nutrient and phytoplankton dynamics on Georges Bank. Marine Ecology Progress Series 228, 57–74.

Townsend, D.W., Keller, M.D., Sierachi, M.E., Ackleson, S.G., 1992. Spring phytoplankton blooms in the absence of vertical water column stratification. Nature 360, 59–62.

Werner, D., 1977. The Biology of Diatoms. University of California Press, California, 498pp.

Wiebe, P., Beardsley, R., Mountain, D., Bucklin, A., 2002. US GLOBEC Northwest Atlantic/Georges Bank Program. Oceanography 15, 13–29.

Yoshie, N., Yamanaka, Y., Kishi, M.J., Saito, H., 2003. One dimensional ecosystem model simulation of the effects of vertical dilution by the winter mixing on the spring diatom bloom. Journal of Oceanography 59, 563–571.